Propranolol and parathyroid hormone synergistically improve bone volume fraction by suppressing resorption

Annika Treyball, BA[1^], Audrey C. Bergeron, MS[1^], Daniel J. Brooks, MS[2], Kathleen T. Nevola, MS[1,3], Hina Hashmi, BS[1], Kenichi Nagano, DDS, PhD[4], Deborah Barlow[5], Karen L. Houseknecht, PhD[5], Roland Baron, DDS, PhD[4], Mary L. Bouxsein, PhD[2], Anyonya R. Guntur, PhD[1,6], Katherine J. Motyl, PhD[1,6,7]*

[1]Center for Molecular Medicine, Maine Medical Center Research Institute, Scarborough, ME
[2]Center for Advanced Orthopaedic Studies, Beth Israel Deaconess Medical Center, Boston, MA
[3]Tufts Graduate School of Biomedical Sciences, Tufts University, Boston, MA
[4]Department of Oral Medicine, Infection and Immunity, Harvard School of Dental Medicine, Boston, MA
[5]Department of Pharmacology, University of New England, Biddeford, ME
[6]Graduate School of Biomedical Sciences and Engineering, University of Maine, Orono, ME
[7]Tufts University School of Medicine, Tufts University, Boston, MA

^*Annika Treyball and Audrey Bergeron have been assigned co-first authorship.*

Current Affiliations

- Annika Treyball is presently affiliated with the Tufts University School of Medicine.
- Hina Hashmi is presently affiliated with the College of Osteopathic Medicine, University of New England.
- Kenichi Nagano is presently affiliated with the Department of Oral Pathology and Bone Metabolism, Institute of Biomedical Sciences, Nagasaki University.

**Address correspondence to:*
Katherine J. Motyl
81 Research Drive
Scarborough, ME 04074
(207) 396-8004
motylk@mmc.org

Conflict of Interest Statement:
The authors have declared that no conflict of interest exists.

Abstract

Although the non-selective β-blocker, propranolol, improves bone density with PTH treatment in mice, the mechanism of this effect is unclear. To address this, we used a combination of *in vitro* and *in vivo* approaches to address how propranolol influences bone remodeling in the context of PTH treatment. *In vitro*, propranolol amplified the acute, PTH-induced, intracellular calcium signal and elevated *Igf1* expression in osteoblasts. *In vivo,* intermittent PTH and propranolol had synergistic effects in the trabecular bone of the distal femur. The most striking finding was a complete suppression of PTH-induced bone resorption. Despite this, PTH-induced receptor activator of nuclear factor kappa-B ligand (RANKL) mRNA and protein levels were unaltered by propranolol. Interestingly, propranolol suppressed differentiation of primary osteoclasts, suggesting a novel direct influence of propranolol on osteoclasts *in vivo*. Taken together, this work suggests combining propranolol with PTH could be beneficial to patients with extremely low bone density.

Introduction

The sympathetic nervous system (SNS) plays a critical role in the regulation of bone remodeling. The SNS suppresses bone formation and promotes receptor activator of nuclear factor kappa-B ligand (RANKL)-mediated osteoclast recruitment, resulting in low trabecular bone volume fraction in mice (Elefteriou et al., 2005; Takeda et al., 2002). Consistent with this, tyrosine hydroxylase, one of the enzymes involved in norepinephrine production, is present in nerves within bone, marrow, and periosteum (Mach et al., 2002). The major adrenergic receptor mediating downstream effects of norepinephrine appears to be the β2AR in mice (Takeda et al., 2002). Deletion of β2AR, or treatment with the non-selective βAR antagonist (β-blocker) propranolol, prevents bone loss in situations of stress, antipsychotic and antidepressant treatment, and in other situations in which sympathetic signaling to bone may be elevated (Motyl et al., 2015, 2013; Ortuno et al., 2016; Takeda et al., 2002; Yadav et al., 2009; Yirmiya et al., 2006). The majority of studies point toward a mechanism of β2AR suppressing bone formation directly in the osteoblast, and activating bone resorption indirectly, through the RANKL/OPG pathway (Ducy et al., 2000; Elefteriou et al., 2005; Takeda et al., 2002). Indeed, mice with an osteoblast-specific deletion of *Adrb2* have a high bone density phenotype as adults, with increased bone formation and reduced *Rankl* expression (Kajimura et al., 2011). However, some studies have found evidence for direct effects of β2AR signaling in osteoclasts (Kondo et al., 2013; Rodrigues et al., 2012), suggesting the downstream effects of elevated SNS activity may be more complex than generally accepted.

Despite this complexity, identifying osteoporosis treatment strategies that modulate sympathetic signaling remains clinically useful. β-blockers are one such class of drugs that has been shown to reduce fracture risk and increase BMD in patients (Yang et al., 2012)(Toulis et

al., 2014). Furthermore, rodent studies have shown that combining β-blockers with teriparatide (intermittent truncated parathyroid hormone, PTH) may further promote bone density, but any benefit of combined treatment has not been examined in humans. Evidence from ovariectomized mice suggests that combining PTH treatment with propranolol increases bone mineral density beyond the levels achieved by PTH alone, and histomorphometric analyses indicated that improvement was largely due to increased bone formation and osteoblast number (Pierroz et al., 2006). Recent literature also suggests that PTH-induced bone formation may be at the expense of bone marrow adiposity since osteoblasts and adipocytes arise from a common mesenchymal progenitor (Fan et al., 2017). Furthermore, propranolol has been shown to inhibit marrow adipocyte differentiation, which could, in turn, enhance osteogenesis (Baek et al., 2014). Despite this, how combined PTH and propranolol treatment influences marrow adiposity remains unknown and may be important for understanding the mechanism of improved bone formation with combined treatment.

On a cellular level, evidence from *in vitro* and *in vivo* studies suggest that PTH efficacy is dependent upon the presence of the β2AR. Deletion of *Adrb2,* the gene that encodes β2AR, prevents the anabolic effect of intermittent PTH in young and aged mice, suggesting some β2AR signaling is required (Hanyu et al., 2012). One mechanism of this may be through β2AR signaling allowing G-protein βγ (Gβγ) subunit to bind endosomal PTH1R, which sustains cAMP levels leading to enhanced mineralization in osteoblasts (Jean-Alphonse et al., 2017). cAMP signaling, however, is not the only avenue for PTH effects to be transduced to the cell (Gesty-Palmer and Luttrell, 2011)(Cheloha et al., 2015). PTH1R also signals through phospholipase C to increase Ca^{2+} release from intracellular stores, as well as through arrestin-mediated mechanisms (Gesty-Palmer and Luttrell, 2011)(Cheloha et al., 2015). There is an established role

for intracellular Ca^{2+} signaling in the regulation of osteoblast differentiation through the calmodulin/CamKII pathway regulating AP-1 and CREB/ATF4 transcription factors (Zayzafoon et al., 2005). It has been shown that silencing of *Adrb2* can increase pCREB (Moriya et al., 2015), but it remains unknown whether combination of PTH treatment with β2AR antagonists would impact these pathways.

To further investigate the cellular and systemic effects of co-modulation of PTH1R and β2AR, we performed a series of *in vitro* and *in vivo* assays pharmacologically targeting these receptors. A pharmacological approach was chosen so that any advantages of combination treatments may eventually be translated to humans. Briefly, we determined that the β-blocker propranolol enhanced PTH-induced Ca^{2+} signaling in osteoblast-like cells *in vitro* and that the combination of PTH and propranolol *in vivo* synergistically increased bone volume fraction in the distal femur in part by increasing markers of bone formation. More striking, however, was that propranolol prevented PTH-induced bone resorption, but did not impact PTH-induced changes in RANKL or OPG pathway members. Finally, we identified that this effect may be through direct anti-osteoclastogenic effects of propranolol. In all, these findings suggest that modifications to PTH therapy that mimic outcomes from propranolol treatment, or simply combining PTH with β-blockers, may be a useful approach to minimizing resorption and promoting net bone accrual.

Results

PTH-induced intracellular calcium signaling is enhanced by propranolol

To test the impact of β-blockers on PTH-induced calcium signaling in osteoblasts, we first measured the concentration-dependence of the intracellular Ca^{2+} response to PTH in MC3T3-E1 cells differentiated for 7 days (Figure 1A). PTH induced a measurable Ca^{2+} signal at concentrations as low as 10 nM and the peak response was observed at 1 μM. Using a log transformation, we calculated the concentration with 50% of maximal excitation to be 66.64 nM. Therefore, we used a concentration of 100 nM in our studies, to be within the dynamic range of the concentration-response curve, but also within range of previous reports. Next, we found that pre-treatment with propranolol significantly increased the intracellular Ca^{2+} signal induced from PTH (Figure 1B, C).

To determine whether combined PTH and propranolol treatment had any functional consequence in osteoblasts, we examined gene expression after acute treatment with PTH, propranolol or both. Although there were no differences in early osteoblastogenic markers *Runx2* and *Sp7* (not shown), PTH induced *Osteocalcin* expression (main effect of PTH p=0.016) similarly in both vehicle and propranolol treated cells, although only the group treated with PTH alone (no propranolol present) reached pairwise statistical significance (Figure 1D, E). Because intracellular Ca^{2+} has been shown to modulate AP-1 family transcription factors, we examined gene expression of *Fos.* Interestingly, the PTH-induced increase in *Fos* was higher when propranolol was present (Figure 1F), consistent propranolol promoting PTH-induced intracellular Ca^{2+} levels. One established mechanism of osteoanabolism from PTH is through increased expression and autocrine signaling of IGF-1 (Esen et al., 2015). We found a significant increase in *Igf1* expression only in the PTH and propranolol co-treated group (Figure 1G). These findings

Figure 1

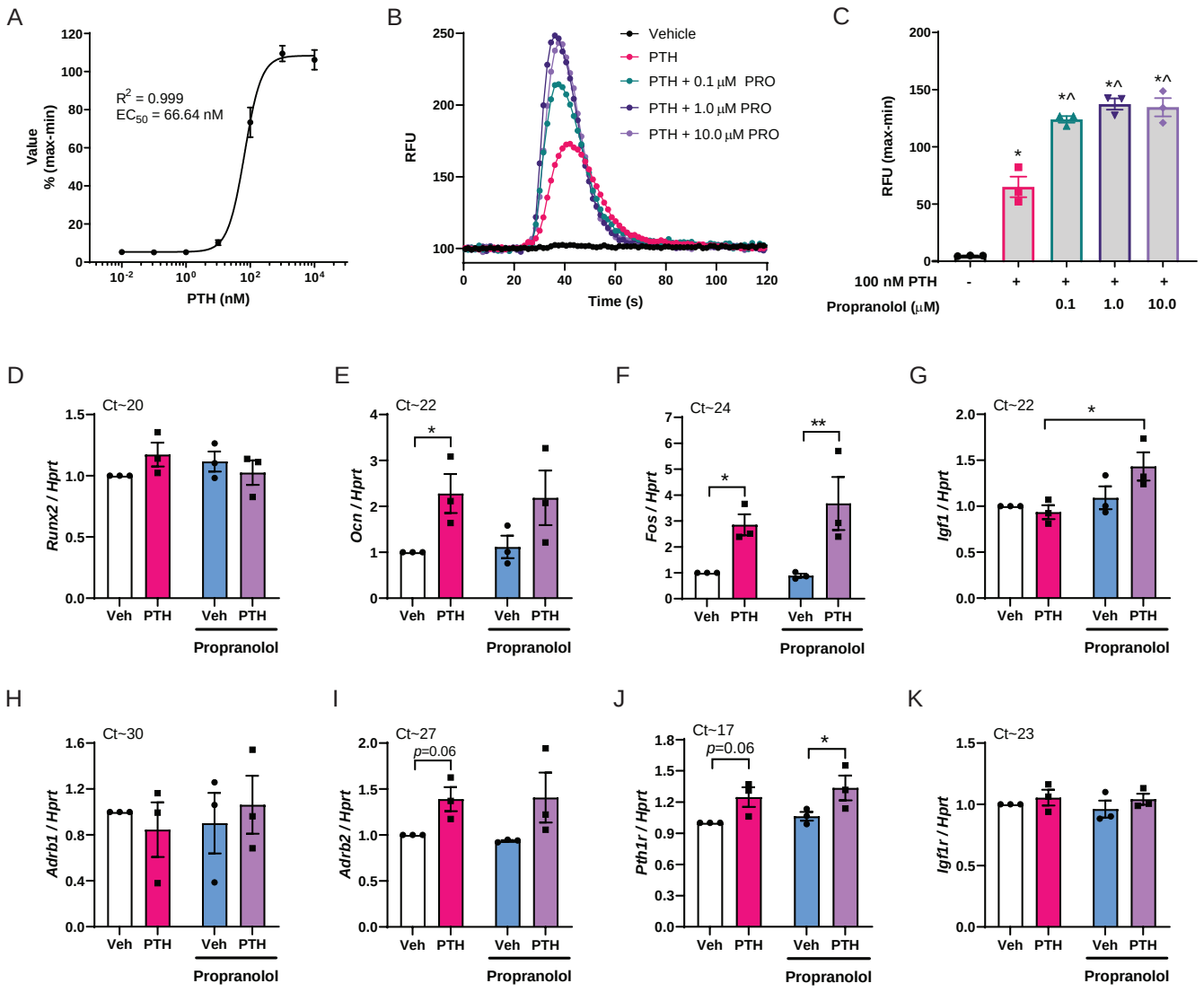

Figure 1. β-blocker propranolol potentiated osteoblast intracellular Ca^{2+} and *Igf1* expression. MC3T3-E1 cells were differentiated to day 7 in osteogenic media. (A) Fluorescence ratio indicative of intracellular Ca^{2+} concentrations was expressed as a percentage of the maximum level. (B) Representative traces of 100 nM PTH-induced fluorescence over time with pretreatment of vehicle, or 0.1, 1 or 10 μM propranolol. (C) Quantification of the maximum-minimum PTH-induced Ca^{2+} fluorescence after pretreatment with vehicle or propranolol. One representative of three experiments (each performed in triplicate) is shown. *p<0.05 compared to vehicle-treated (black), ^p<0.05 compared to 100 nM PTH-treated (pink) by Tukey's post-hoc test after significant one-way ANOVA. (D-K) Gene expression of *Runx2*, *Ocn*, *Fos*, *Igf1*, *Adrb1*, *Adrb2*, *Pth1r* and *Igf1r* in MC3T3-E1 cells at day 7 after 1 hour treatment with vehicle (white), 100 nM PTH (pink), 1 μM propranolol (blue) or 100 nM PTH + 1 μM propranolol (purple). Genes are normalized to non-modulated housekeeping gene, *Hprt*. Each data point represents the mean from an independent experiment, performed in triplicate. Expression levels in vehicle-treated cells from each experiment were set to 1. Approximate Ct values of vehicle-treated groups are shown above each graph. Bars represent mean of the three independent experiments ± SEM. *p<0.05, **p<0.01 by Holm-Sidak post hoc test after a significant two-way ANOVA.

suggest propranolol may improve bone formation from PTH through increasing intracellular Ca^{2+} signaling and promoting expression of *Igf1*.

To ensure the relevant receptors were present in MC3T3-E1 cells at day 7 of differentiation, we also examined *Adrb1, Adrb2, Pth1r* and *Igf1r* (Figure 1, H-K). *Adrb1* expression was low and variable, but *Adrb2* was more highly expressed and there was a trend toward increased expression with PTH treatment. Furthermore, both *Pth1r* and *Igf1r* were highly expressed and the expression levels of *Pth1r* also increased with PTH treatment, reaching statistical significance in the propranolol treated group. Thus, co-treatment with propranolol appears to promote PTH-induced Ca^{2+} flux, as well as *Igf1* and *Pth1r* expression. It is well-established that long-term PTH treatment *in vitro* does not model the *in vivo* anabolic effects of intermittent PTH therapy. Therefore, to test whether these acute effects had long-term consequences we moved to *in vivo* studies.

Propranolol improved total BMD in the presence of PTH

To test whether propranolol would improve PTH-induced bone formation, we treated mice with either vehicle, PTH, propranolol, or PTH + propranolol from 16-20 weeks of age. Neither body weight, fat mass, nor fat-free mass was altered in any of the treatment groups, suggesting that any bone changes would be independent of differences in loading (Table I). As expected, PTH had a significant main effect on total and femoral aBMD and aBMC (Table I). Although propranolol only had a significant main effect on total aBMD, all bone parameters measured by DXA were highest in the PTH + propranolol group (Table I). Interestingly, co-treatment with PTH and propranolol increased total aBMD beyond that caused by PTH or propranolol alone.

Table I. Body composition and areal bone parameters from mice treated with PTH and/or propranolol.

	Vehicle (N=10)	PTH (N=11)	Propranolol (N=9)	PTH + Propranolol (N=11)	2-way ANOVA *p*-values		
					PTH	Propranolol	Interaction
Body Mass (g)	21.8 ± 0.5	22.5 ± 0.4	21.7 ± 0.3	22.6 ± 0.4	*ns*	*ns*	*ns*
Lean Mass (g)	17.4 ± 0.4	17.9 ± 0.3	18.0 ± 0.3	17.9 ± 0.3	*ns*	*ns*	*ns*
Fat Mass (g)	2.6 ± 0.1	2.5 ± 0.2	2.6 ± 0.2	2.7 ± 0.2	*ns*	*ns*	*ns*
Total aBMD (g/cm^2)	0.0527 ± 0.0003	0.0544 ± 0.0004**	0.0535 ± 0.0004	0.0559 ± 0.0003^##	<0.01	<0.01	*ns*
Femur aBMD (g/cm^2)	0.0620 ± 0.0006	0.0655 ± 0.0008	0.0628 ± 0.0016	0.0678 ± 0.0008##	<0.01	*ns*	*ns*
Total aBMC (g)	0.438 ± 0.006	0.463 ± 0.006	0.444 ± 0.007	0.475 ± 0.009#	<0.01	*ns*	*ns*
Femur aBMC (g)	0.0097 ± 0.0002	0.0102 ± 0.0003	0.0093 ± 0.0003	0.0105 ± 0.0002##	<0.01	*ns*	*ns*

*p<0.05, **p<0.01 compared to vehicle group.

^p<0.05, ^^p<0.01 compared to PTH group.

#p<0.05, ##p<0.01 compared to propranolol group.

PTH and propranolol had site-specific effects on trabecular bone microarchitecture

To investigate the impact of PTH and propranolol treatment on bone microarchitecture, we performed μCT on L5 vertebrae and femurs. Propranolol and PTH both independently improved trabecular BV/TV of the L5 vertebra, but the combination of PTH and propranolol improved BV/TV and BMD above and beyond that of either treatment alone (Figure 2). This is likely due to a combined effect of increased trabecular thickness and increased trabecular number, the latter of which was only significantly increased by PTH when propranolol was present. Consistent with this, PTH and propranolol together significantly reduced BS/BV ratio compared to propranolol alone (Figure 2).

In the distal femur, we focused our examination of PTH and propranolol effects on two distinct sites, the primary and secondary spongiosa (Figure 3). In the secondary spongiosa, PTH increased Tb. BV/TV, BMD, and Conn.D and these parameters were all increased further by combined treatment with propranolol (Figure 3B-D). Although some parameters (Tb.N, Tb.Th, Tb.Sp, and BS/BV) were not altered by PTH alone, the combination reduced SMI, Tb.Sp, and BS/BV, while significantly increasing Tb.N and Tb.Th (Figure 3E-I). The primary spongiosa also had striking changes from PTH, including increased BV/TV, BV and BMD (Figure 3J-L), but these were not exacerbated or diminished by combination PTH and propranolol treatment. Tissue mineral density (TMD), a measurement of the density of the bone itself (not including any marrow), was suppressed with PTH treatment, suggesting that mineral deposition may be compromised (Figure 3M). Interestingly, however, propranolol significantly elevated TMD in PTH-treated mice such that is was not different from vehicle-treated (Figure 3M). This indicates the quality of mineralization in the primary spongiosa during combination PTH and propranolol treatment may be improved compared to PTH alone.

Figure 2

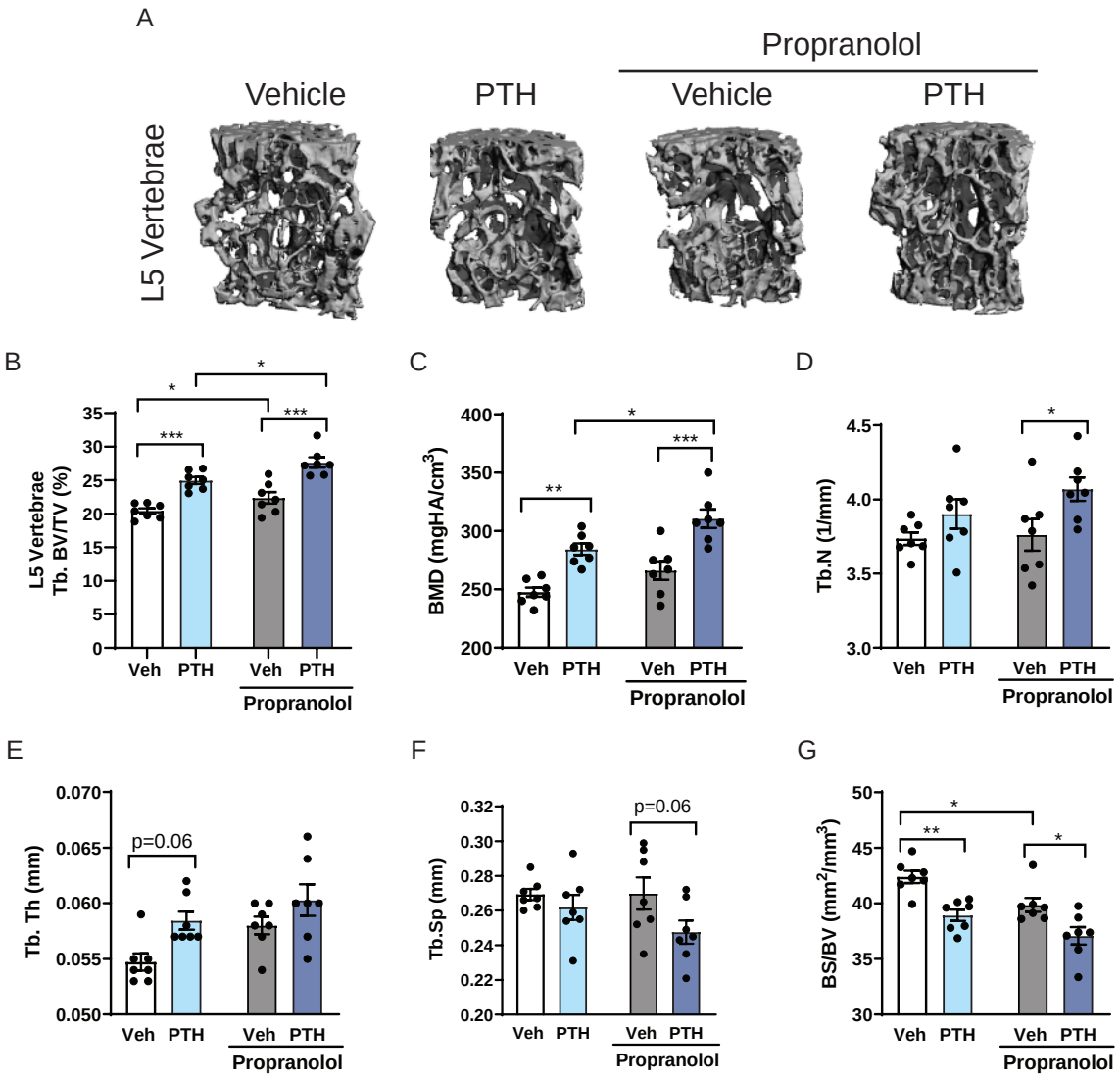

Figure 2. Propranolol improved the positive effects of PTH on trabecular bone in the L5 vertebrae. Mice were treated with vehicle (white), 80 µg/kg PTH (light blue), 0.5 mg/ml propranolol (gray), or PTH and propranolol (dark blue) for 4 weeks, from 16-20 weeks of age. (A) Representative µCT images from L5 vertebrae. (B-G) Trabecular bone volume fraction (Tb. BV/TV), bone mineral density (BMD), number (Tb.N), thickness (Tb.Th), separation (Tb.Sp), and bone surface/bone volume (BS/BV). Bars represent mean +/- standard error. *p<0.05, **p<0.01 by Holm-Sidak post hoc test after a significant two-way ANOVA.

Figure 3

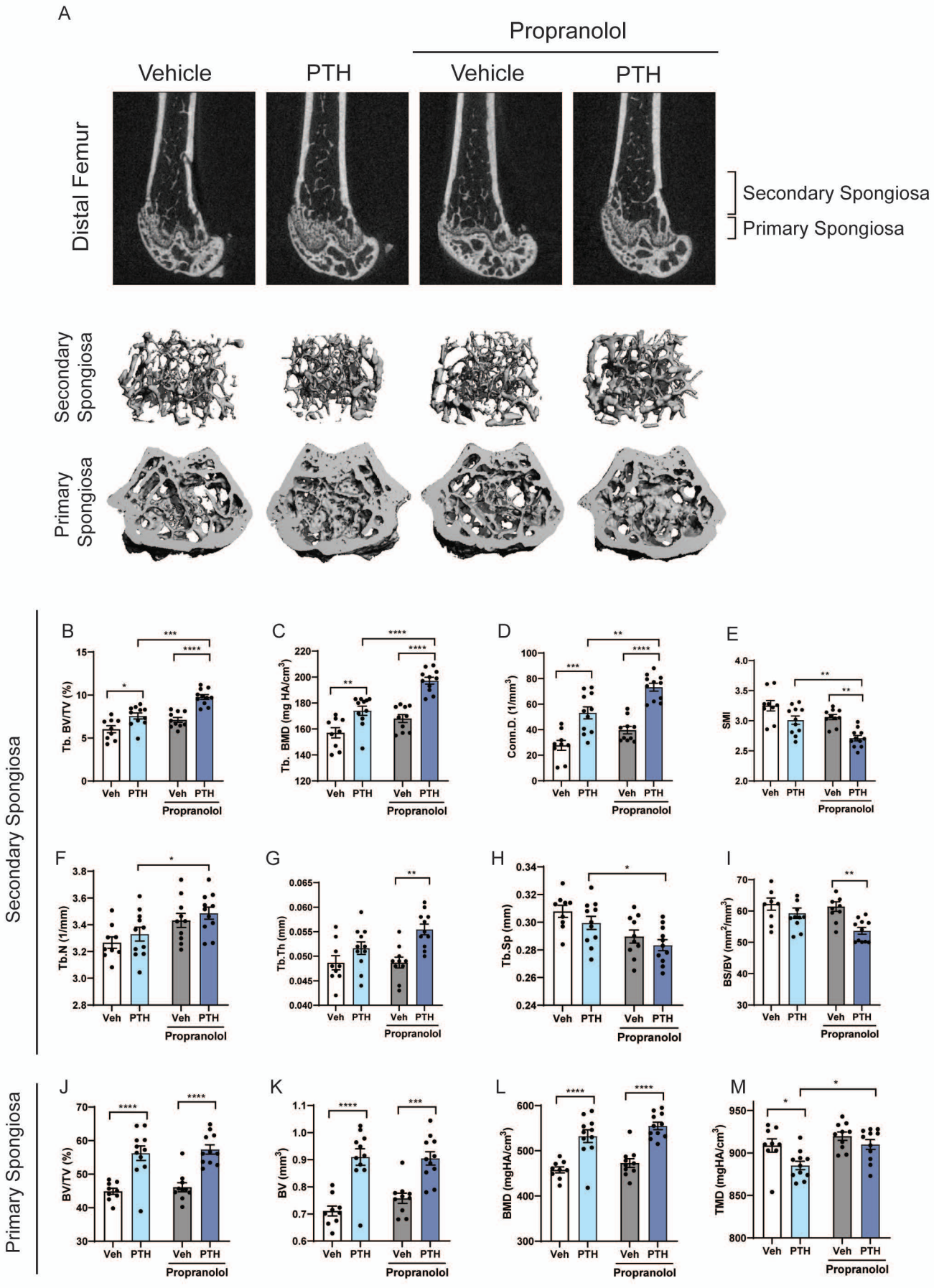

Figure 3. Trabecular bone in the femur secondary spongiosa is enhanced by combination PTH and propranolol treatment. Mice were treated with vehicle (white), 80 μg/kg PTH (light blue), 0.5 mg/ml propranolol (gray), or PTH and propranolol (dark blue) for 4 weeks, from 16-20 weeks of age. (A) Representative 2D (top) and 3D (bottom) images of trabecular micro architecture in the primary and secondary spongiosa of the distal femur. (B-I) Trabecular microarchitectural parameters from the secondary spongiosa. (J-K) Volumetric and densitometric measurements from the primary spongiosa. Bars represent mean +/- standard error. *p<0.05, **p<0.01, ***p<0.001, ****p<0.0001 by Holm-Sidak post hoc test after a significant two-way ANOVA.

Cortical bone microarchitecture

PTH significantly increased cortical area (Ct.Ar) and polar moment of inertia (pMOI) in the femur midshaft, but did not significantly impact marrow area (Ma.Ar), total area (Tt.Ar), cortical thickness (Ct.Th), tissue mineral density (TMD) or porosity (Figure 4 A-H). Although propranolol treatment did not impact these parameters on its own, propranolol significantly improved the effect of PTH on the cortical bone such that Ct.Ar, Ct.Ar/Tt.Ar, Ct.Th and TMD were elevated in the PTH + propranolol group compared to propranolol alone (Figure 4A, D, E, and F). The increased Ct.Ar/Tt.Ar with combination treatment is most likely due to a reduction in Ma.Ar, because Tt.Ar was clearly unchanged (Figure 4B-D).

Propranolol promoted bone formation in PTH-treated mice.

To determine whether co-treatment with propranolol modulated the effect of PTH on bone formation, we performed serum, histomorphometric, and mRNA analyses to evaluate bone remodeling activity. As expected, PTH increased the serum marker of bone formation, P1NP, and this was further increased by co-treatment with PTH and propranolol (Figure 5A). Histomorphometric analyses in the L5 vertebrae indicated a significant effect of PTH by 2-way ANOVA on MAR and BFR parameters (Figure 5B, C). Similarly, osteoblast parameters were elevated by PTH, but were not significantly modulated by the combination with propranolol. However, propranolol did not have a significant main effect on these parameters (except to decrease the N.Ob/B.Pm) and, when combined with PTH, did not increase these indices beyond the level of PTH alone (Figure 5B, C). Propranolol did, however, reduce the amount of OS/BS in PTH-treated mice (Figure 5C).

Figure 4

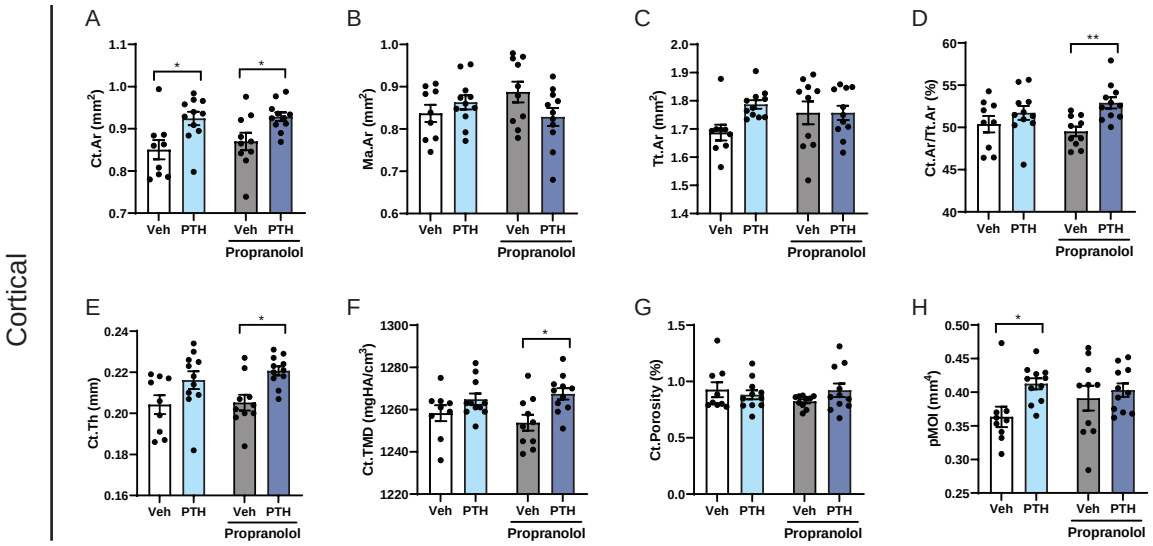

Figure 4. Propranolol improved cortical thickness and density in PTH-treated mice. Mice were treated with vehicle (white), 80 µg/kg PTH (light blue), 0.5 mg/ml propranolol (gray), or PTH and propranolol (dark blue) for 4 weeks, from 16-20 weeks of age. (A-H) Cortical bone microarchitectural parameters, cortical area (Ct.Ar), marrow area (Ma.Ar), total area (Tt.Ar) cortical area fraction (Ct.Ar/Tt.Ar), cortical thickness (Ct.Th), cortical tissue mineral density (Ct.TMD), cortical porosity, and polar moment of inertia (pMOI) were analyzed at the midshaft of the femur. Bars represent mean +/- standard error. *p<0.05, **p<0.01 by Holm-Sidak post hoc test after a significant two-way ANOVA.

Figure 5

A

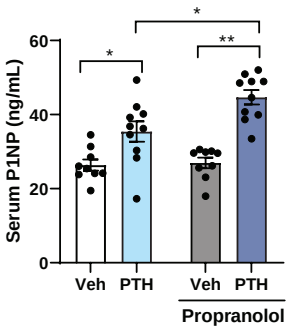

B

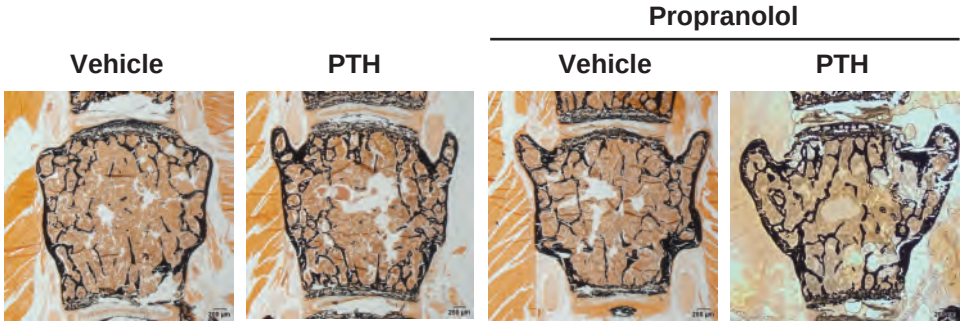

C

	Vehicle (N=7)	PTH (N=7)	Propranolol (N=7)	PTH + Propranolol (N=9)	2-way ANOVA *p*-values		
					PTH	Propranolol	Interaction
BV/TV (%)	9.4 ± 0.8	14.0 ± 0.9**	10.3 ± 0.9	15.6 ± 0.4$^{\#\#}$	<0.01	*ns*	*ns*
Tb.Th (µm)	37.5 ± 1.7	43.5 ± 2.1*	39.0 ± 1.6	45.0 ± 1.5$^{\#}$	<0.01	*ns*	*ns*
Tb.N (mm^{-1})	2.5 ± 0.1	3.2 ± 0.1**	2.6 ± 0.2	3.5 ± 0.1$^{\#\#}$	<0.01	*ns*	*ns*
Tb.Sp (µm)	376 ± 20	273 ± 14**	349 ± 24	246 ± 8$^{\#\#}$	<0.01	*ns*	*ns*
MAR (µm/day)†	1.19 ± 0.07	1.65 ± 0.07**	1.12 ± 0.13	1.65 ± 0.07$^{\#\#}$	<0.01	*ns*	*ns*
MS/BS (%)†	38.3 ± 2.1	42.3 ± 2.2	39.8 ± 3.3	37.3 ± 4.1	*ns*	*ns*	*ns*
BFR/BV (%/day)†	2.58 ± 0.21	3.61 ± 0.36	2.21 ± 0.26	3.08 ± 0.50	0.01	*ns*	*ns*
BFR/TV (%/day)†	0.23 ± 0.02	0.45 ± 0.05*	0.25 ± 0.05	0.46 ± 0.09$^{\#}$	<0.01	*ns*	*ns*
BFR/BS (µm^3/µm^2/day)†	0.45 ± 0.04	0.70 ± 0.06*	0.45 ± 0.06	0.62 ± 0.08	<0.01	*ns*	*ns*
N.Ob/B.Pm (mm^{-1})	14.7 ± 1.0	22.5 ± 1.5**	12.4 ± 0.6	19.4 ± 1.2$^{\#\#}$	<0.01	0.03	*ns*
N.Ob/T.Ar (mm^{-2})	71.1 ± 8.5	147.7 ± 6.5**	64.4 ± 3.7	127.0 ± 7.9$^{\#\#}$	<0.01	*ns*	*ns*
Ob.S/B.Pm (%)	17.4 ± 1.2	26.8 ± 1.8**	14.8 ± 0.8	24.2 ± 1.4$^{\#\#}$	<0.01	*ns*	*ns*
OS/BS (%)	14.1 ± 1.2	18.8 ± 2.0	13.3 ± 1.3	12.5 ± 1.2^^	*ns*	0.02	*ns*
O.Th (µm)	2.69 ± 0.13	3.14 ± 0.14	2.71 ± 0.27	2.76 ± 0.12	*ns*	*ns*	*ns*

*p<0.05 compared to vehicle, **p<0.01 compared to vehicle

^p<0.05 compared to PTH, ^^p<0.01 compared to PTH

$^{\#}p$<0.05 compared to PRO, ##p<0.01 compared to PRO

†N=4-5 for dynamic measurements.

D E F G H

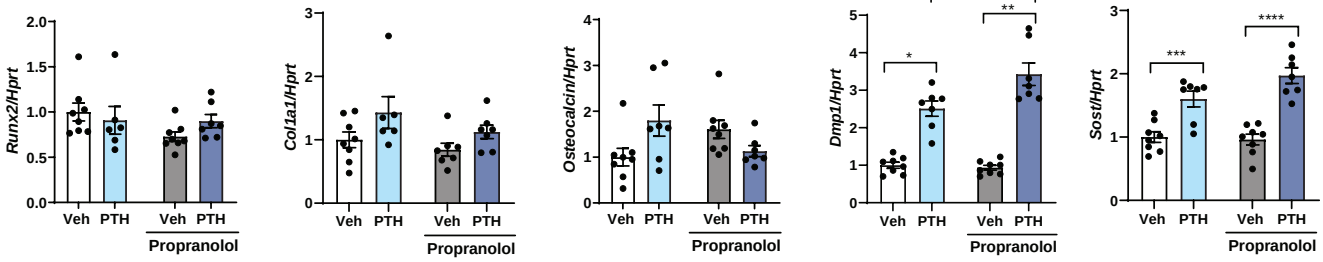

Figure 5. Propranolol improved bone formation markers in PTH-treated mice. Mice were treated with vehicle (white), 80 µg/kg PTH (light blue), 0.5 mg/ml propranolol (gray), or PTH and propranolol (dark blue) for 4 weeks, from 16-20 weeks of age. (A) Serum P1NP was measured by ELISA. (B-C) Static and dynamic histomorphometry representative images and quantification of architectural, bone formation and osteoblast parameters measured in L5 vertebrae. (D-H) Gene expression of markers of bone formation and osteoblast maturity were analyzed in the tibia and normalized by the non-modulated housekeeping gene, *Hprt*. Bars represent mean +/- standard error. *p<0.05, **p<0.01 by Holm-Sidak post hoc test after a significant two-way ANOVA.

In general, these findings contrast the serum P1NP finding. Therefore, we examined mRNA markers of osteoblastogenesis and osteocyte maturation in the tibia. Although we did not see significant differences in *Runx2*, *Col1a1*, or *Osteocalcin* expression (Figure 5D-F), we did observe differences in late osteoblast and osteocyte markers. First, dentin matrix acidic phosphoprotein 1 (*Dmp1*) expression was increased with PTH treatment, but there was also a significant interaction ($p=0.01$) such that PTH-induced *Dmp1* expression was higher in the propranolol treated group, while propranolol alone had no effect in the absence of PTH (Figure 5G). Surprisingly, intermittent treatment with PTH induced *Sost* expression, in contrast to previously reported effects with chronic elevation, and *Sost* was elevated to a greater degree in propranolol treated mice (Figure 5H) (Bellido et al., 2005). Although serum P1NP is elevated, changes in bone formation (histological and mRNA-based) do not convincingly explain the improved BV/TV in mice treated with PTH and propranolol.

Bone marrow adipocytes

Recent studies have suggested PTH may suppress bone marrow adipose tissue (BMAT) as a means or consequence of promoting bone formation. Although marrow adipocyte size was not influenced by PTH, there was a significant interaction effect ($p<0.05$) of PTH and propranolol in both adipocyte volume / total volume (AV/TV) and adipocyte number parameters. In particular, PTH tended to reduce marrow adipocyte numbers in mice not treated with propranolol ($p=0.08$) but this effect was blunted in propranolol-treated mice (Figure S1).

PTH-induced osteoclast differentiation and activity was blocked by propranolol

Figure S1

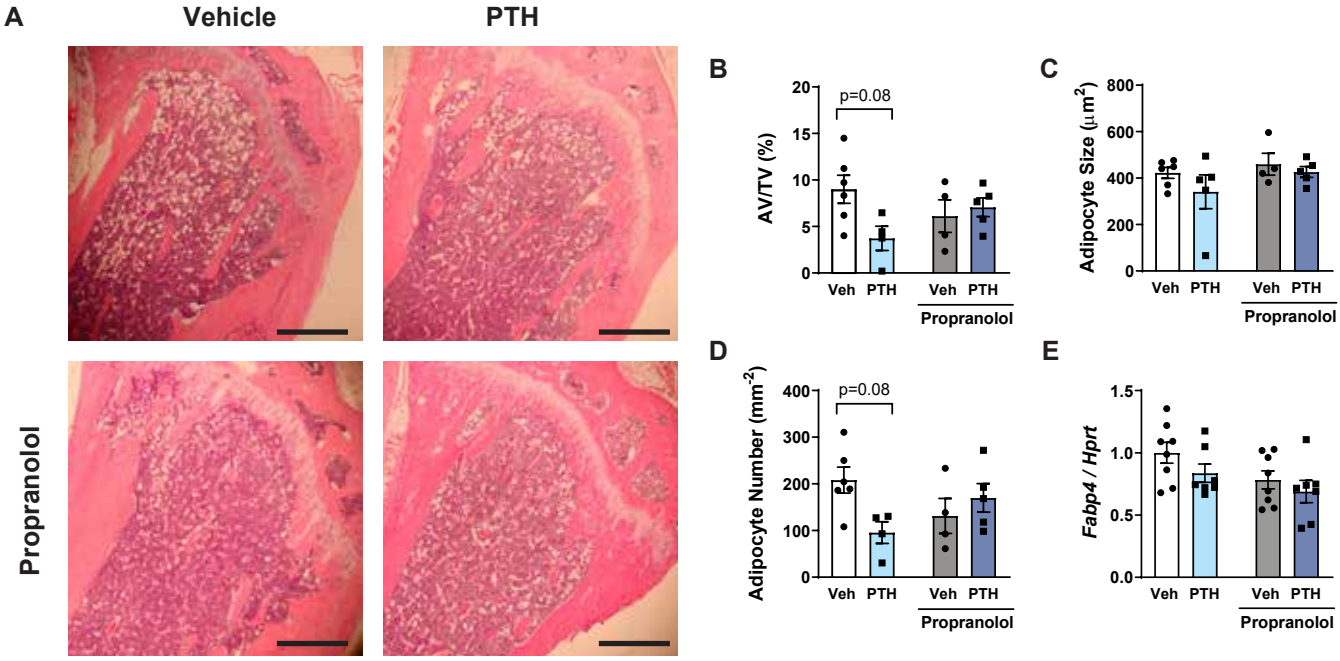

Consistent with the known effect of PTH to increase resorption, PTH increased expression of *Ctsk* and *Trap5*, as well as the serum protein levels of the resorption marker CTx (Figure 6A-C). Interestingly, propranolol prevented the PTH-induced increase in *Trap5* expression and serum CTx, suggesting propranolol prevents PTH-induced resorption (Figure 6B, C). Consistent with the literature, histomorphometry indicated that PTH increased the number of osteoclasts (N.Oc/T.Ar, Figure 6D). Propranolol alone did not have any impact on the number of osteoclasts or the other osteoclast parameters (Figure 6D). When combined, however, the number of osteoclasts (N.Oc/B.Pm and N.Oc/T.Ar) and the osteoclast surface fraction (Oc.S/BS) was lower in mice treated with PTH and propranolol compared to those treated with PTH alone (Figure 6D), interaction $p \leq 0.02$). Notably, the PTH-induced increase in N.Oc/T.Ar was completely blocked by co-treatment with propranolol ($p<0.01$, Figure 6D). All three lines of evidence related to osteoclasts (serum, mRNA, and histomorphometry) point toward a strong effect of propranolol to reduce PTH-induced bone resorption.

Propranolol can centrally suppress sympathetic activity, therefore we measured norepinephrine (NE) levels in serum as well. While neither PTH nor propranolol independently modulated NE, the combination treatment resulted in significantly lower circulating NE compared to PTH alone (Figure 6E), suggesting a systemic lowering of sympathetic signaling by propranolol might be responsible for the suppressed resorption. Because the current understanding of the mechanism of NE signaling-induced osteoclastogenesis is through the modulation of *receptor activator of nuclear factor kappa-B ligand* (*Rankl*) expression in the osteoblast, we measured circulating RANKL and found that, to our surprise, propranolol had no effect on PTH-induced RANKL levels (Figure 6F). Furthermore, although PTH induced *Rankl* gene expression in cortical bone as expected, propranolol did not have any blunting effect on

Figure 6

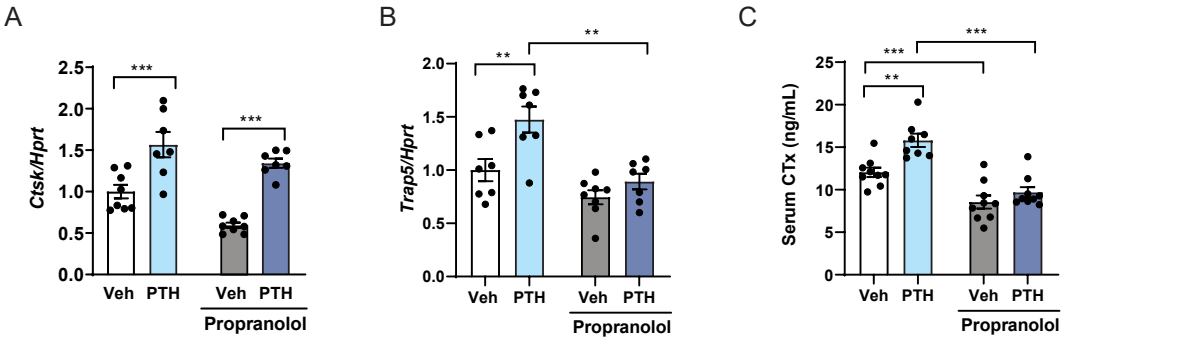

D

	Vehicle (N=7)	PTH (N=7)	Propranolol (N=7)	PTH + Propranolol (N=9)	2-way ANOVA *p*-values		
					PTH	Propranolol	Interaction
N.Oc/B.Pm (mm^{-1})	5.9 ± 0.3	6.2 ± 0.2	5.3 ± 0.4	4.2 ± 0.2#,^^	*ns*	<0.01	0.02
N.Oc/T.Ar (mm^{-2})	28.2 ± 2.4	41.3 ± 2.4**	27.4 ± 1.9	27.7 ± 1.5^^	<0.01	<0.01	<0.01
Oc.S/B.Pm (%)	14.8 ± 0.8	15.9 ± 0.5	13.1 ± 0.9	10.6 ± 0.5^^	*ns*	<0.01	0.02
ES/BS (%)	5.9 ± 0.5	5.8 ± 0.4	5.0 ± 0.7	4.1 ± 0.3^	*ns*	0.01	*ns*
*p<0.05 compared to vehicle, **p<0.01 compared to vehicle							
^p<0.05 compared to PTH, ^^p<0.01 compared to PTH							
#p<0.05 compared to PRO, ##p<0.01 compared to PRO							

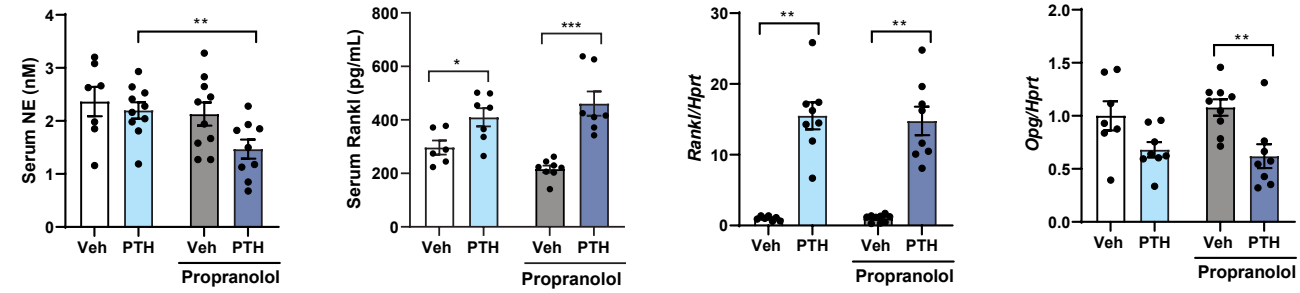

Rankl (Figure 6G), but did lower *Opg* (Figure 6H), suggesting other mechanisms were responsible for the reduced osteoclast numbers and CTx levels in PTH and propranolol treated mice.

Propranolol directly inhibits osteoclast differentiation and function

Because propranolol blocked resorption *in vivo* without modulating the RANKL/OPG pathway members we examined, we hypothesized that osteoclasts may respond directly to propranolol. We first accessed publicly available microarray data from RAW264.7 cells treated for 48 hours with RANKL and vehicle. The detection levels of *Adrb1* and *Adrb3* were only slightly higher or equivalent to those of *Bglap* and *Mcsf,* which are not expressed in osteoclasts, suggesting *Adrb1* and *Adrb3* had little to no detectable expression (Figure 7A). *Adrb2* was detected at a higher level, comparable to the amount of *Ctsk* before RANKL addition. However, *Adrb2* levels were not as high as other classically expressed osteoclast genes (*Cfms*, *Nfat1*), and were not changed with RANKL addition (Figure 7A). Next, we examined mRNA levels of adrenergic receptors in bone marrow cells differentiated to osteoclasts in our hands (Figure 7B). Consistent with the RAW264.7 cell data, *Adrb2* was more highly expressed (Ct values are lower) than *Adrb1* (Figure 7B).

βARs have some agonist-independent signaling, and β-blockers can act as inverse agonists to reduce this signaling, so we treated primary bone marrow cells with propranolol while undergoing osteoclast differentiation. We examined the influence of 0.1, 1.0 and 10 μM propranolol at day 7, when osteoclast differentiation has plateaued. In a concentration-dependent manner, propranolol significantly reduced the number of multinucleated TRAP-positive cells (Figure 7C, D), as well as reduced the hydroxyapatite area resorbed (Figure 7E, F). To ensure

Figure 7

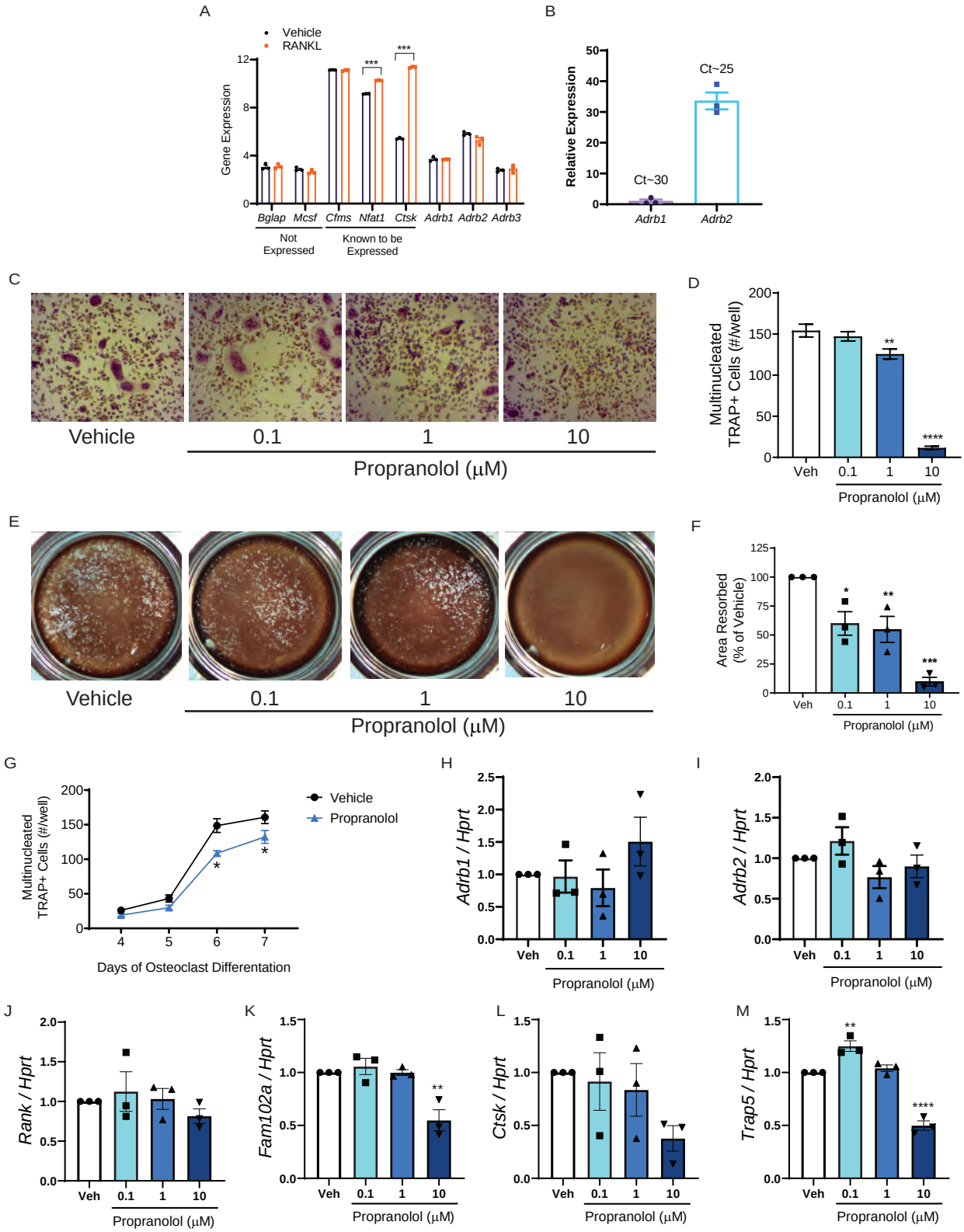

Figure 7. Osteoclast differentiation is impaired with propranolol treatment *in vitro*. (A) Publicly available microarray data from GEO, including *Adrb1*, *2* and *3*, as measured in RAW264.7 cells after 48-hour treatment with vehicle or RANKL. n=3/group. ***p<0.001 by Student's t-test. (B) Expression levels of *Adrb1* and *Adrb2* in primary bone marrow-derived osteoclasts. n=3. (C) Representative images of TRAP-stained osteoclasts that were differentiated in the presence of vehicle or 0.1, 1, or 10 μM propranolol. (D) One representative of four independent experiments where TRAP positive osteoclasts were counted in 96-well plates. (E) Representative OsteoAssay Surface plates stained for phosphate with a Von Kossa stain. White areas indicate surface that was resorbed by osteoclasts. (F) Quantification of three independent experiments, where the vehicle control for each was set to 100%. (D and F) *p<0.05, **p<0.01, ****p<0.0001 by Tukey's post hoc test after a significant one-way ANOVA. (G) Time course of primary bone marrow-derived osteoclast differentiation in the presence of vehicle or 1 μM propranolol. N=8 replicates per time point. *p<0.05 by Holm-Sidak post hoc test after a significant two-way ANOVA. (H-M) Gene expression normalized to housekeeping gene *Hprt* in primary osteoclasts treated with vehicle or indicated concentrations of propranolol. n=3 independent experiments with the vehicle control from each experiment set to 1. (H-M) *p<0.05, **p<0.01, ****p<0.0001 by Tukey's *post hoc* test after a significant one-way ANOVA. Bars represent mean +/- standard error.

that we were targeting an appropriate time point, we tested how 1.0 μM propranolol influenced differentiation over time. Between days 5 and 6, there was a large increase in the number of multinucleated, TRAP-positive osteoclasts, and this was attenuated with 1 μM propranolol (Figure 7G). The difference between vehicle and propranolol treated number of osteoclasts remained significant at day 7.

Expression of *Adrb1* and *Adrb2* were unchanged with increasing concentrations of propranolol (Figure 7H, I). *Rank, Rela, Fos* and *Nfatc1,* genes involved with osteoclast differentiation at earlier stages, were not affected by treatment with propranolol (Figure 7J and not shown). However, consistent with the staining and resorption assays, propranolol dose-dependently reduced gene expression of several key mid- to late-stage osteoclastogenic genes and markers, including, *Fam102a, Ctsk*, and *Trap5* (Figure 7K-M), although *Ctsk* was too variable to be called significant. Taken together, these findings suggest that propranolol directly suppresses later stage osteoclast differentiation and function via β2AR.

Discussion

Here we show that propranolol and intermittent PTH co-treatment causes an improvement in bone microarchitecture that exceeds that seen in intermittent PTH treatment alone, which is consistent with previous co-treatment studies (Pierroz et al., 2006). We add to this, however, the novel findings that propranolol enhances tissue mineral density, which may be through promoting Ca^{2+} signaling pathway in osteoblasts. We are also the first to show that propranolol prevents PTH-induced resorption and that this may be through direct inhibition of osteoclast differentiation. In the absence of β-blockers, intermittent PTH treatment promotes both bone formation *and* resorption, which could be of concern to individuals with severely lowered bone density and/or high levels of resorption. Intracortical remodeling, which may lead to fracture, has been associated with serum PTH levels in humans, as well as with daily intermittent PTH treatment in rabbits (Osima et al., 2018; Zebaze et al., 2017). Nonetheless, PTH is very effective at building new bone, so bone loss that occurs from heightened resorption needs to be weighed against its anabolic activity. Our findings suggest that combining PTH with propranolol or other β-blockers may be an attractive option to prevent unwanted bone loss in patients with very low BMD.

The mechanism of propranolol action on bone to prevent resorption is likely in part through direct effects of propranolol on osteoclasts. Neither PTH-induced serum RANKL nor *Rankl* gene expression was suppressed by propranolol, despite clear improvement in trabecular microarchitecture of the distal femur and the suppressed markers of resorption. The majority of publications point toward osteoblast expression of RANKL as being the major mediator in the effects of the sympathetic nervous system on osteoclasts (Elefteriou et al., 2005; Kajimura et al., 2011). However, our findings suggest that this is not the same mechanism through which

propranolol blocks resorption. In studies examining the osteoblast-mediated mechanism of SNS-induced bone loss, some experiments suggested no effect of *Adrb2* in osteoclasts. For example, Elefteriou et al. elegantly showed that the non-specific βAR agonist isoproterenol only induces osteoclast differentiation in osteoblast and bone marrow macrophage (BMM) co-cultures when wildtype but not *Adrb2*$^{-/-}$ osteoblasts are present (Elefteriou et al., 2005). Similarly, the effect of isoproterenol to induce osteoclast differentiation is not dependent upon the genotype of the BMMs (Elefteriou et al., 2005). These data, in combination with findings from models with osteoblast-specific deletions of *Adrb2*, have led to the generally accepted tenet that osteoblasts are the sole mediators of the SNS effect on bone, including the mediators of osteoclast recruitment (Kajimura et al., 2011).

There is a relative scarcity of literature examining the effects of β-adrenergic signaling directly in osteoclasts. Rodrigues, et al. showed that propranolol prevented osteoclastogenesis of RAW 264.7 cells through suppression of NFATc1 protein expression, as well as later markers of differentiation: *Acp5, Ctsk,* and *Mmp9* (Rodrigues et al., 2012). This suggests a role for βAR signaling in controlling NFATc1, which is under the control of calcium-calmodulin and calcineurin signaling. Kondo, et al. demonstrated that isoproterenol enhanced osteoclastogenesis in bone marrow macrophages and RAW 264.7 cells by increasing reactive oxygen species (Kondo et al., 2013). Our findings are more aligned with these reports because we show expression of *Adrb2* in primary bone marrow-derived osteoclasts, as well as a direct effect of propranolol to suppress osteoclast differentiation. Although this is consistent with the other *in vitro* reports, this mechanism remains to be established *in vivo*.

Despite the paucity of literature relating to the effects of the SNS in osteoclasts directly, there is extensive evidence that *Adrb2* is expressed in other cells of the myeloid lineage and that

the SNS plays a role in their function (De Angelis et al., 2019). Indeed, the SNS is important for the innate immune response required for tissue repair but can be pathologically activated during certain conditions, such as in heart failure. β-blockers are a common therapeutic for heart failure and they work in part by reducing inflammatory cytokine levels (De Angelis et al., 2019). Systemic suppression of inflammation may also be an interesting, yet unexplored, avenue to investigate the mechanism of efficacy of β-blockers in improving BMD, especially with regards to resorption.

In contrast to our findings, global knockout of β2AR prevents any anabolic action of PTH by preventing the PTH-induced increase in mineral apposition and osteoclast number (Hanyu et al., 2012). Although these findings are paradoxical in some sense, they suggest that a basal level of β2-adrenergic signaling in bone may be required for PTH action. It is also clear that pharmaceutical inhibition of β2AR with propranolol is mechanistically distinct from the disruption of signaling through genetic deletion. Propranolol can act as an inverse agonist, meaning it has effects inhibitory toward cAMP signaling even when no agonist is present, reducing spontaneous β2AR receptor activity (Baker, 2003). Furthermore, propranolol also binds to the lesser expressed β1AR and is known to have non-specific effects, including acting as a weak antagonist to some serotonin receptors, which could, in turn, impact bone remodeling (Sozzani et al., 1992; Tinajero et al., 1993).

Moriya et al. showed that *Adrb2* knockdown enhances PTH-induced phosphorylation of CREB, suggesting a suppressive function of β2AR on PTH action (Moriya et al., 2015). This is consistent with our findings that PTH effects in osteoblasts are enhanced with pharmacological β2AR inhibition. Some intracellular scaffolding proteins, such as members of the Na^+/H^+ exchange regulatory cofactor (NHERF) family, selectively promote coupling of the PTH1R to

the $G\alpha_q$-PLC-β signaling pathway(Cheloha et al., 2015). NHERF also couples β2AR to the cytoskeleton, and agonist binding causes uncoupling from the cytoskeleton (Wheeler et al., 2007). It is unknown, however, whether propranolol might uncouple β2AR from NHERF, G proteins and/or the other signaling components, which could lead to the enhanced PTH-induced Ca^{2+} flux (Figure 1B, C). Nonetheless, we observed enhanced *Igf1* expression after co-treatment in osteoblasts, which has previously been shown work in an autocrine manner to stimulate aerobic glycolysis in osteoblasts in response to PTH-treatment at 6 hours (Esen et al., 2015). In our hands, elevation of *Igf1* after 1 hour of propranolol treatment suggests an acceleration of this timetable, which may lead to the improved PTH effect on bone formation and tissue mineral density that we observed *in vivo.*

TMD in the primary spongiosa was significantly higher with PTH and propranolol co-treatment compared to PTH alone (Figure 3M). A similar trend was seen with cortical TMD (Figure 4F) as well as total areal BMD assessed by DXA (Table I). Serum P1NP also indicated global increases in bone formation with the combined treatment (Figure 5A), but this was not observed in dynamic histomorphometric measurements of mineral apposition or bone formation in the trabecular bone of the L5 vertebra (Figure 5C). However, gene expression in cortical bone of the tibia suggested more mature osteoblasts/osteocytes (Figure 5G, H), indicating that propranolol may have site-specific effects. Further studies investigating the mineral properties of bone exposed to both PTH and propranolol would be necessary to determine if this combination of treatments may improve strength in patients and animal models.

Clinical literature suggests that β-blockers prevent bone loss and reduce fracture risk in humans. Yang et al. reported that β-blocker use was associated with a 17% decrease in risk of fractures (Yang et al., 2012). Toulis et al. analyzed 16 studies involving over 1.5 million subjects

and found that the risk of fracture was significantly reduced (by 15%) in subjects receiving β-blockers as compared to control subjects, independent of sex, fracture site, or dose (Toulis et al., 2014). In contrast to what is the apparent mechanism in rodent models, β1-selective blockers were found to be more effective at reducing fractures than non-selective β-blockers (i.e. propranolol). More recently, when evaluating adrenergic receptor mRNA expression in human bone biopsies, Khosla et al. found that ADRB1 and ADRB2, but not ADRB3, were expressed in human bone (Khosla et al., 2018). Additionally, patients treated with β1-selective blockers had better bone microarchitecture by quantitative computed tomography (qCT) than non-users, had reduced CTx levels compared to placebo-treated patients, and had increased BMD at the ultradistal radius, but these results were not seen in propranolol (non-selective β-blockers) treated patients. Overall, this data suggests that β1-selective blockers are more protective against decreased BMD and increased risk of fracture than non-selective β-blockers. Whether the perceived difference between rodents and humans is due to β1AR being understudied in rodent models or due to an actual species-specific difference in the relative importance of β1AR vs β2AR in bone remains unclear.

Our findings reinforce the work of others suggesting that β-blockers, which are routinely used clinically, may be an effective treatment or co-treatment for osteoporosis. Importantly, here we showed that propranolol prevented resorption without modulating PTH-induced RANKL, suggesting that the current understanding of the mechanism of β-blocker and sympathetic nervous system action on bone is incomplete. Investigating the mechanisms of these effects, whether through modulating osteoblast function or osteoclasts directly, will be necessary for the accurate interpretation of clinical and preclinical studies examining how the sympathetic nervous system modulates bone homeostasis and contributes to bone pathologies.

411 **Methods**

412 *Osteoblast assays*

413 MC3T3-E1 (clone 4) cells were purchased from ATCC and maintained at a low passage number
414 in α-MEM containing 1% penicillin streptomycin (P/S) and 10% fetal bovine serum (FBS). For
415 calcium assays, cells were plated overnight in 96-well black wall plates at a density of $5x10^4$
416 cells/well. Cells were then differentiated for 7 days with ascorbic acid and β-glycerophosphate as
417 previously described (Motyl et al., 2017). PTH (H-1660, Bachem) was aliquoted and stored in
418 glass vials at -70°C as a 10^{-4} M stock in 4 mM HCl supplemented with 0.1% bovine serum
419 albumin. PTH was thawed and diluted immediately prior to use. Propranolol hydrochloride
420 (P0884, Sigma-Aldrich) was dissolved in 1x HBSS buffer containing 20 mM HEPES for each
421 experiment. Calcium assays were performed with the FLIPR Calcium 6 Assay Kit (Molecular
422 Devices) according to the manufacturer's protocol. In brief, on day 7 of differentiation, cells
423 were incubated with calcium dye for two hours at 37°C and 5% CO_2. Then, fluorescence was
424 measured on a FlexStation 3 Multi-Mode Microplate Reader using SoftMax Pro 7 software
425 (Molecular Devices) in kinetic mode in response to additions of a range of concentrations of
426 PTH. Change in relative fluorescence units (maximum – minimum) is indicative of intracellular
427 calcium (iCa^{2+}) levels. Concentration-dependent change in max-min value was plotted on a
428 logarithmic scale and fit with a 4-parameter logistic curve to calculate the EC_{50}. In some
429 experiments, calcium dye incubation was concurrent with pretreatment with propranolol.
430 Additional 24-well plates were treated simultaneously with PTH and propranolol for 1 hour,
431 without the Calcium 6 reagents, and were saved for mRNA analyses.

432

433 *Mice and drug treatment*

Sixteen-week-old C57BL/6J (Jackson Laboratories, Bar Harbor, ME) female, intact mice underwent baseline body weight measurements and were randomly assigned to one of four treatment groups. Female mice were chosen because of their higher propensity to have an anabolic response to intermittent PTH. Mice were treated with either vehicle, PTH, propranolol or both PTH and propranolol. PTH aliquots were generated as above and thawed and diluted in 0.9% saline immediately prior to injection. Vehicle and PTH (80 μg/kg) were administered by subcutaneous injection five days per week for four weeks. Propranolol hydrochloride oral solution (West-Ward Pharmaceuticals) was dissolved in drinking water at a concentration of 0.5 mg/mL and was delivered daily for four weeks to animals in the propranolol and PTH + propranolol groups as described (Motyl et al., 2015). At 20 weeks-of-age, mice were sacrificed one hour after treatment and tissues were either fixed in 10% buffered formalin or snap-frozen in liquid nitrogen and stored at -70°C. A similar study was conducted with just 5 days of treatment to obtain additional samples for some mRNA and serum analyses and are identified in the figure legends.

Dual-energy X-ray absorptiometry (DXA)

Mice underwent DXA measurements at baseline and at 20 weeks of age for fat-free mass, fat mass, bone mineral density, and bone mineral content using the PIXImus dual-energy X-ray densitometer (GE-Lunar, Madison, WI). The instrument was calibrated daily with a mouse phantom provided by the manufacturer. Mice were anesthetized with isoflurane and placed ventral side down with each limb and tail positioned away from the body. Full body scans were obtained, and X-ray energy absorptiometry data were gathered and processed with manufacturer-

456 supplied software (Lunar PIXImus 2, version 2.1). The head was specifically excluded from all
457 analyses due to concentrated mineral in skull and teeth.
458
459 *Micro-computed tomography* (µCT)
460 A high-resolution desktop micro-tomographic imaging system (µCT40, Scanco Medical AG,
461 Bruttisellen, Switzerland) was used to assess the microarchitecture of the fifth lumbar (L5)
462 vertebral body and the femur in accordance with published guidelines (Bouxsein and Boyd,
463 2010). All analyses were performed using the Scanco Evaluation software.
464 In the L5 vertebra, scans were acquired using a resolution of 10 μm^3, 70 kVp peak x-ray tube
465 potential, 114 mA x-ray tube current, 200 ms integration time, and were subjected to Gaussian
466 filtration and segmentation. The endocortical region of the vertebral body was manually selected
467 beginning 100 µm inferior to the cranial growth plate and extending to 100 µm superior to the
468 caudal growth plate. Trabecular bone was segmented from soft-tissue using a threshold of 460
469 $mgHA/cm^3$. Measurements included trabecular bone volume fraction (Tb.BV/TV, %), trabecular
470 thickness (Tb.Th, mm), trabecular number (Tb.N, mm^{-1}), trabecular separation (Tb.Sp, mm),
471 connectivity density (Conn.D, mm^{-3}), and trabecular bone mineral density (Tb.BMD,
472 $mgHA/cm^3$).
473 To address microarchitecture in the primary and secondary spongiosa of the distal femur and
474 the cortical bone of the femur midshaft, scans were acquired with the same parameters used for
475 the L5 vertebrae. The primary spongiosa region of interest started at the peak of the distal growth
476 plate and extended proximally for 500 µm (50 transverse slices) and included the whole cross-
477 section of the bone. The secondary spongiosa region of interest started immediately superior to
478 the primary spongiosa region and extended 1500 µm (150 transverse slices) proximally and

included the endocortical region of the bone. In both regions, bone was segmented from soft-tissue using a mineral density threshold of 460 mgHA/cm^3. Trabecular bone in the endocortical area of the secondary spongiosa region was analyzed for bone volume fraction (Tb.BV/TV, %), trabecular thickness (Tb.Th, mm), trabecular number (Tb.N, mm^{-1}), trabecular separation (Tb.Sp, mm), connectivity density (Conn.D, mm^{-3}), and trabecular bone mineral density (Tb.BMD, mgHA/cm^3). The bone in the primary spongiosa was analyzed for bone volume, total volume, and bone mineral density.

Cortical bone architecture was analyzed in a 500 µm long region at the femoral mid-diaphysis (55% of the total femur length inferior to the top of the femoral head). Cortical bone was segmented from soft tissue using a threshold of 700 mgHA/cm^3. Measurements included cortical bone area (Ct.Ar, mm^2), total cortical cross-sectional area (Tt.Ar, mm^2), cortical bone area fraction (Ct.Ar/Tt.Ar, %), cortical thickness (Ct.Th, mm) and cortical porosity (%).

Histology and Histomorphometry

Tibiae were fixed in 10% neutral-buffered formalin and transferred to 70% ethanol after 24 hours. Samples were decalcified, paraffin-embedded, sectioned, and stained with hematoxylin and eosin. Adipocyte size and number in the marrow in the region of the secondary spongiosa were analyzed with BIOQUANT OSTEO software (BIOQUANT Image Analysis Corporation, Nashville, TN). Total adipocyte area was divided by total area (marrow plus trabecular bone) in the secondary spongiosa and multiplied by 100 to calculate adipocyte volume / total volume (AV/TV). Adipocyte number was normalized to the total area measured.

Vertebrae were fixed in 10% neutral-buffered formalin and transferred to 70% ethanol after 24 hours. The fixed lumbar vertebrae (L2-L5) were dehydrated with acetone and embedded

in methylmethacrylate. Undecalcified 4-µm-thick sections were obtained by microtome and stained with Von Kossa method for showing the mineralized bone. The consecutive second section was left unstained for the analysis of fluorescence labeling and the third section was stained with 2% Toluidine Blue (pH 3.7) for the analysis of osteoblasts, osteoid, and osteoclasts. The bone histomorphometric analysis was performed in the lumbar vertebra under 200X magnification in a 1.35 mm high x 1.3 mm wide region where was located 400 µm away from the upper and lower growth plate using OsteoMeasure analyzing software (Osteometrics Inc., Decatur, GA), in accordance with published guidelines (Dempster et al., 2013). The structural parameters (BV/TV, Tb.Th, Tb.N, and Tb.Sp) were obtained by taking an average from two different analysis of consecutive sections. The structural, dynamic and cellular parameters were calculated and expressed according to the standardized nomenclature (Dempster et al., 2013).

Enzyme Immunoassays

Serum concentrations of amino-terminal propeptide of type 1 procollagen (P1NP), cross-linked C-telopeptide (CTx) and TNF-related activation-induced cytokine (RANKL) were measured with the Rat/Mouse P1NP enzyme immunoassay (EIA), RatLaps EIA (both from Immunodiagnostic Systems, Scottsdale, AZ), and the Quantikine ELISA Mouse TRANCE/RANKL/TNSFSF11 Kit (R&D Systems, Minneapolis, MN). The intraassay variations were 6.3%, 6.9% and 4.3%, and the interassay variations were 8.5%, 12% and 6.9% respectively. All measurements were performed in duplicate.

RNA isolation and real-time PCR (qPCR)

524 Total RNA was isolated from whole tibia and cortical shell using the standard TRIZOL (Sigma,
525 St. Louis, MO) method. Total RNA from cells was isolated using an RNeasy Mini Kit (Qiagen).
526 cDNA was synthesized using the High Capacity cDNA Reverse Transcriptase Kit (Applied
527 Biosystems, Foster City, CA) according to the manufacturer's instructions. mRNA expression
528 analysis was performed using an iQ SYBR Green Supermix or Taqman Gene Expression Assays
529 with an iQ5 thermal cycler and detection system (Bio-Rad, Hercules, CA). Hypoxanthine
530 guanine phosphoribosyl transferase (*Hprt*) was used as an internal standard control
531 gene(Vengellur and LaPres, 2004). Primer sequences are listed in the supplemental information
532 (Table S1).
533
534 *Norepinephrine extraction and measurements*
535 A volume of 20 µL of serum was combined with 100 µL of HPLC grade acetonitrile and vortex
536 mixed for two minutes. Subsequent to centrifugation at 14000 rpm for five minutes, the
537 supernatant was transferred to a 96-well plate for liquid chromatograph tandem mass
538 spectrometry (LC/MS-MS) analysis. A calibration curve was formed in mouse plasma from
539 0.305-2500 nM by serial dilution and extracted via the same methodology. An Agilent 1200
540 system consisting of a binary pump, column compartment and autosampler was used for solvent
541 delivery and sample introduction. Chromatographic separation was performed on a Phenomenex
542 Hydro RP 2.0 x 150 mm 4 µm column via a gradient using 0.1% formic acid in water (A) and
543 0.1% formic acid in acetonitrile (B). Gradient elution was 98% A from 0-1 minute, ramping to
544 50% A from 1.1 to 3.0 minutes, holding at 50% until 5.5 minutes, with re-equilibration at initial
545 conditions from 5.6 to 7.5 minutes. The flow rate was 0.30 mL/min, and column temperature was
546 30°C. Detection of norepinephrine was obtained using an Agilent 6460 triple quadrupole mass

Supplemental Table

Table SI. qPCR primer information.

Target Gene	Source/Supplier	Sequence	Catalog Number	Reference
Adrb1	Qiagen (Germantown, MD)	Not provided	330001, PPM05035A	N/A
Adrb2	Qiagen (Germantown, MD)	Not provided	330001, PPM04265A	N/A
Col1a1	Primer Design (Southampton, UK)	Forward: 5'-TCG TGG CTT CTC TGG TCT C-3' Reverse: 5'-CCG TTG AGT CCG TCT TTG C-3'	N/A	N/A
Ctsk	IDT (Coralvile, IA)	Forward: 5'-GCA GAG GTG TGT ACT ATG-3' Reverse: 5'-GCA GGC GTT GTT CTT ATT-3'	N/A	N/A
Dmp1	IDT (Coralvile, IA)	Forward: 5'-TCG CTG AGG TTT TGA CCT TGT-3' Reverse: 5'-CTC ACT GTT CGT GGG TGG TG-3'	N/A	(Motyl et al., 2015)
Fabp4	IDT (Coralvile, IA)	Forward: 5′-GCG TGG AAT TCG ATG AAA TCA-3′ Reverse: 5′-CCC GCC ATC TAG GGT TAT GA-3′	N/A	(Li et al., 2003)
Fos	Qiagen (Germantown, MD)	Not provided	330001, PPM02940C	N/A
Hprt	IDT (Coralvile, IA)	Forward: 5′-AAG CCT AAG ATG AGC GCA AG-3' Reverse: 5′-TTA CTA GGC AGA TGG CCA CA-3′	N/A	(Vengellur and LaPres, 2004)
Igf1	Primer Design (Southampton, UK)	Forward: 5'-GAC CGA GGG GCT TTT ACT TC-3' Reverse: 5'TGC TTT TGT AGG CTT CAG TGG-3'	N/A	N/A
Opg	IDT (Coralvile, IA)	Forward: 5'GAAGAAGATCATCCAAGACATTGAC-3' Reverse: 5'-TCCATAAACTGAGTAGCTTCAGGAG-3'	N/A	(Irwin et al., 2013)
Osteocalcin (Bglap)	IDT (Coralvile, IA)	Forward: 5'-ACG GTA TCA CTA TTT AGG ACC TGT-3' Reverse: 5'-ACT TTA TTT TGG AGC TGC TGT GAC-3'	N/A	(Ontiveros and McCabe, 2003)
Pth1r	IDT (Coralvile, IA)	Forward: 5'-TTT CCC GGT GCC TTC TCT TTC-3' Reverse: 5'-CAG GCG CAA TGT GAC AAG C-3'	N/A	(Ide et al., 2018)
Rankl	Primer Design (Southampton, UK)	Forward: 5'-TTT GCA CAC CTC ACC ATC AAT-3' Reverse: 5'- CCC TTA GTT TTC CGT TGC TTA AC-3'	N/A	N/A
Runx2	IDT (Coralvile, IA)	Forward: 5'-GAC AGA AGC TTG ATG ACT CTA AAC C-3' Reverse: 5'-TCT GTA ATC TGA CTC TGT CCT TGT G-3'	N/A	(Ontiveros et al., 2004)
Sost	Qiagen (Germantown, MD)	Not provided	330001, PPM36047A	N/A
Trap5 (Acp5)	IDT (Coralvile, IA)	Forward: 5'-AAT GCC TCG ACC TGG GA-3' Reverse: 5'-CGT AGT CCT CCT TGG CTG CT-3'	N/A	(Wiren et al., 2004)

spectrometer, monitoring the transition 152.0 → 107.0 with a fragmentor of 94 V and a collision energy of 18 V. The retention time of norepinephrine was 1.37 minutes.

Microarray Analyses

Publicly available microarray data from RAW264.7 cells treated for 48 hours with RANKL and vehicle was accessed from GEO (Gene Expression Omnibus, accession number GSE74847) (Takigawa et al., 2016). Gene expression values were obtained after log2-transformation and normalization to the Robust Multiarray Average (RMA).

Osteoclast culture

Primary osteoclasts were isolated from bone marrow from 6-8 week old female mice, as previously described(Motyl et al., 2012). Briefly, bone marrow was plated and cultured with 30 ng/mL M-CSF and 50 ng/mL RANKL containing propranolol or vehicle for 6-7 days. Osteoclasts were fixed in glutaraldehyde and stained for TRAP (387A-1KT, Sigma-Aldrich), then TRAP-positive osteoclasts with 3 or more nuclei were counted. Corning OsteoAssay Surfaces were stained for Von Kossa and resorbed area was quantified with ImageJ as previously described(DeMambro et al., 2012). Additional osteoclasts cultured on plastic were saved for mRNA analyses at day 7.

Sample size estimation and statistics

Sample size for mouse experiments was estimated based on previous experiments in our laboratory using trabecular BV/TV as a primary outcome. Secondary outcomes of interest included serum and histomorphometric indices of bone remodeling. All statistics were performed

with Prism 7 statistical software (GraphPad Software, Inc., La Jolla, CA). Results were analyzed for statistically significant differences using one-way or two-way ANOVA followed by Tukey's or Holm-Sidak multiple comparison *post hoc* tests, where appropriate. Statistical significance was set at $p < 0.05$. All data are expressed as the mean ± standard error of the mean (SEM). Outliers were handled as follows: first, any scientific/biological reason for the outlier was investigated (i.e. sick mouse, degraded RNA, bad histology section); second, if no explanation for the outlier was found we performed an outlier test to determine if the datum was > 3 standard deviations (SD) from the mean of the other samples in that group. If the datum was > 3 SD from the mean, it was excluded from further analysis. Outlier handling did not significantly change the interpretation of the results.

Study Approval

The Institutional Animal Care and Use Committee of the Maine Medical Center Research Institute approved all mouse protocols.

Author Contributions

AT was responsible for experimental design, data acquisition, data analysis, interpretation, and drafting of the manuscript. ACB was responsible for experimental design, data acquisition, data analysis, interpretation, drafting and critical review of the manuscript. DJB was responsible for data acquisition, data analysis, interpretation, drafting of and critical revision of the manuscript. HH was responsible for data acquisition, data analysis, interpretation and drafting of the manuscript. KTN was responsible for data analysis, drafting and critical review of the manuscript. KN was responsible for data acquisition, data analysis, interpretation, drafting of and critical revision of the manuscript. DB was responsible for data acquisition, interpretation, drafting and critical revision of the manuscript. KLH was responsible for experimental design, data interpretation, drafting and critical revision of the manuscript. RB was responsible for data interpretation and critical revision of the manuscript. MLB was responsible for data interpretation and critical revision of the manuscript. ARG was responsible for experimental design, data interpretation and critical revision of the manuscript. KJM was responsible for experimental design, data acquisition, data analysis, interpretation, drafting and critical revision of the manuscript. All authors had final approval of the manuscript.

592 **Acknowledgements**

593 The authors thank Adriana Lelis Carvalho and Audrie L. Langlais for critical evaluation of the
594 work. This work was supported by the National Institute of Arthritis And Musculoskeletal And
595 Skin Diseases (NIAMS) and the National Institute of General Medical Sciences (NIGMS) of the
596 National Institutes of Health (NIH) under award numbers K01AR067858 and P20GM121301 to
597 KJM. This work utilized services of the Maine Medical Center Research Institute (MMCRI)
598 Molecular Phenotyping Core, which is supported by NIH/NIGMS P30GM106391, the
599 Physiology Core, which is supported by NIH/NIGMS P30GM106391 and P20GM121301, the
600 Histopathology and Histomorphometry Core, which is supported by NIH/NIGMS
601 P30GM106391, P20GM121301, and P30103392, and the Mouse Transgenic and In Vivo
602 Imaging Core which is supported by NIH/NIGMS P30GM103392. All cores also received
603 support from the Norther New England Clinical and Translational Research Network
604 NIH/NIGMS U54GM115516. The content is solely the responsibility of the authors and does not
605 necessarily represent the official views of the National Institutes of Health.

606 **Figure Legends**

607 Figure 1. β-blocker propranolol potentiated osteoblast intracellular Ca^{2+} and *Igf1* expression.
608 MC3T3-E1 cells were differentiated to day 7 in osteogenic media. (A) Fluorescence ratio
609 indicative of intracellular Ca^{2+} concentrations was expressed as a percentage of the maximum
610 level. (B) Representative traces of 100 nM PTH-induced fluorescence over time with
611 pretreatment of vehicle, or 0.1, 1 or 10 μM propranolol. (C) Quantification of the maximum-
612 minimum PTH-induced Ca^{2+} fluorescence after pretreatment with vehicle or propranolol. One
613 representative of three experiments (each performed in triplicate) is shown. *p<0.05 compared to
614 vehicle-treated (black), ^p<0.05 compared to 100 nM PTH-treated (pink) by Tukey's *post-hoc*
615 test after significant one-way ANOVA. (D-K) Gene expression of *Runx2, Ocn, Fos, Igf1, Adrb1,*
616 *Adrb2, Pth1r* and *Igf1r* in MC3T3-E1 cells at day 7 after 1 hour treatment with vehicle (white),
617 100 nM PTH (pink), 1 μM propranolol (blue) or 100 nM PTH + 1 μM propranolol (purple).
618 Genes are normalized to non-modulated housekeeping gene, *Hprt*. Each data point represents the
619 mean from an independent experiment, performed in triplicate. Expression levels in vehicle-
620 treated cells from each experiment were set to 1. Approximate Ct values of vehicle-treated
621 groups are shown above each graph. Bars represent mean of the three independent experiments ±
622 SEM. *p<0.05, **p<0.01 by Holm-Sidak *post hoc* test after a significant two-way ANOVA.
623
624 Figure 2. Propranolol improved the positive effects of PTH on trabecular bone in the L5
625 vertebrae. Mice were treated with vehicle (white), 80 μg/kg PTH (light blue), 0.5 mg/ml
626 propranolol (gray), or PTH and propranolol (dark blue) for 4 weeks, from 16-20 weeks of age.
627 (A) Representative μCT images from L5 vertebrae. (B-G) Trabecular bone volume fraction (Tb.
628 BV/TV), bone mineral density (BMD), number (Tb.N), thickness (Tb.Th), separation (Tb.Sp),

629 and bone surface/bone volume (BS/BV). Bars represent mean ± standard error. *p<0.05,
630 **p<0.01 by Holm-Sidak *post hoc* test after a significant two-way ANOVA.
631
632 Figure 3. Trabecular bone in the femur secondary spongiosa is enhanced by combination PTH
633 and propranolol treatment. Mice were treated with vehicle (white), 80 µg/kg PTH (light blue),
634 0.5 mg/ml propranolol (gray), or PTH and propranolol (dark blue) for 4 weeks, from 16-20
635 weeks of age. (A) Representative 2D (top) and 3D (bottom) images of trabecular micro
636 architecture in the primary and secondary spongiosa of the distal femur. (B-I) Trabecular
637 microarchitectural parameters from the secondary spongiosa. (J-K) Volumetric and densitometric
638 measurements from the primary spongiosa. Bars represent mean ± standard error. *p<0.05,
639 **p<0.01, ***p<0.001, ****p<0.0001 by Holm-Sidak *post hoc* test after a significant two-way
640 ANOVA.
641
642 Figure 4. Propranolol improved cortical thickness and density in PTH-treated mice. Mice were
643 treated with vehicle (white), 80 µg/kg PTH (light blue), 0.5 mg/ml propranolol (gray), or PTH
644 and propranolol (dark blue) for 4 weeks, from 16-20 weeks of age. (A-H) Cortical bone
645 microarchitectural parameters, cortical area (Ct.Ar), marrow area (Ma.Ar), total area (Tt.Ar)
646 cortical area fraction (Ct.Ar/Tt.Ar), cortical thickness (Ct.Th), cortical tissue mineral density
647 (Ct.TMD), cortical porosity, and polar moment of inertia (pMOI) were analyzed at the midshaft
648 of the femur. Bars represent mean ± standard error. *p<0.05, **p<0.01 by Holm-Sidak *post hoc*
649 test after a significant two-way ANOVA.
650

651 Figure 5. Propranolol improved bone formation markers in PTH-treated mice. Mice were treated
652 with vehicle (white), 80 µg/kg PTH (light blue), 0.5 mg/ml propranolol (gray), or PTH and
653 propranolol (dark blue) for 4 weeks, from 16-20 weeks of age. (A) Serum P1NP was measured
654 by ELISA. (B-C) Static and dynamic histomorphometry representative images and quantification
655 of architectural, bone formation and osteoblast parameters measured in L5 vertebrae. (D-H)
656 Gene expression of markers of bone formation and osteoblast maturity were analyzed in the tibia
657 and normalized by the non-modulated housekeeping gene, *Hprt*. Bars represent mean ± standard
658 error. *p<0.05, **p<0.01 by Holm-Sidak *post hoc* test after a significant two-way ANOVA.
659
660 Figure 6. Propranolol prevented PTH-induced resorption but not RANKL induction. Mice were
661 treated for 4 weeks (A-F) with vehicle (white), 80 µg/kg PTH (light blue), 0.5 mg/ml propranolol
662 (gray), or PTH and propranolol (dark blue). (A-B) Gene expression of *Ctsk* and *Trap5* was
663 analyzed in the whole tibia and normalized by the non-modulated housekeeping gene, *Hprt*. (C)
664 Serum CTx was measured by ELISA. (D) Histomorphometric analyses of osteoclast and
665 resorption parameters were measured in L5 vertebrae. (E) Serum norepinephrine (NE) was
666 measured by LC/MS/MS. (F) Serum Rankl was measured by ELISA. (G-H) Mice were treated
667 with PTH and/or propranolol for 5 days and cortical shell was collected 1 hour after the last PTH
668 or vehicle dose. Gene expression levels of *Rankl* and *Opg* were normalized to *Hprt*. Bars
669 represent mean ± standard error. *p<0.05, **p<0.01, ***p<0.001 by Holm-Sidak *post hoc* test
670 after a significant two-way ANOVA.
671
672 Figure 7. Osteoclast differentiation is impaired with propranolol treatment *in vitro*. (A) Publicly
673 available microarray data from GEO, including *Adrb1, 2* and *3*, as measured in RAW264.7 cells

after 48-hour treatment with vehicle or RANKL. *n*=3/group. ***p<0.001 by Student's t-test. (B) Expression levels of *Adrb1* and *Adrb2* in primary bone marrow-derived osteoclasts. *n*=3. (C) Representative images of TRAP-stained osteoclasts that were differentiated in the presence of vehicle or 0.1, 1, or 10 μM propranolol. (D) One representative of four independent experiments where TRAP positive osteoclasts were counted in 96-well plates. (E) Representative OsteoAssay Surface plates stained for phosphate with a Von Kossa stain. White areas indicate surface that was resorbed by osteoclasts. (F) Quantification of three independent experiments, where the vehicle control for each was set to 100%. (D and F) *p<0.05, **p<0.01, ****p<0.0001 by Tukey's *post hoc* test after a significant one-way ANOVA. (G) Time course of primary bone marrow-derived osteoclast differentiation in the presence of vehicle or 1 μM propranolol. N=8 replicates per time point. *p<0.05 by Holm-Sidak *post hoc* test after a significant two-way ANOVA. (H-M) Gene expression normalized to housekeeping gene *Hprt* in primary osteoclasts treated with vehicle or indicated concentrations of propranolol. *n*=3 independent experiments with the vehicle control from each experiment set to 1. (H-M) *p<0.05, **p<0.01, ****p<0.0001 by Tukey's *post hoc* test after a significant one-way ANOVA. Bars represent mean ± standard error.

Figure S1. Effects of PTH and propranolol on proximal tibia bone marrow adiposity. Mice were treated for 4 weeks with vehicle (white), 80 μg/kg PTH (light blue), 0.5 mg/ml propranolol (gray), or PTH and propranolol (dark blue). (A) Tibias were decalcified and stained with H & E. Scale bar = 500 μm. (B-D) Adipocyte ghosts were measured using BIOQUANT OSTEO software. (E) *Fabp4* gene expression was measured in whole tibia and normalized to non-modulated housekeeping gene *Hprt.* Bars represent mean ± standard error. Indicated *p*-values

were determined by Holm-Sidak *post hoc* test after a significant interaction effect was found using two-way ANOVA.

References

Baek K, Park HJ, Hwang HR, Baek JH. 2014. Propranolol attenuates calorie restriction- and high calorie diet-induced bone marrow adiposity. *BMB Rep*. doi:10.5483/BMBRep.2014.47.10.176

Baker JG. 2003. Agonist and Inverse Agonist Actions of -Blockers at the Human 2-Adrenoceptor Provide Evidence for Agonist-Directed Signaling. *Mol Pharmacol*. doi:10.1124/mol.64.6.1357

Bellido T, Ali AA, Gubrij I, Plotkin LI, Fu Q, O'Brien CA, Manolagas SC, Jilka RL. 2005. Chronic elevation of parathyroid hormone in mice reduces expression of sclerostin by osteocytes: A novel mechanism for hormonal control of osteoblastogenesis. *Endocrinology*. doi:10.1210/en.2005-0239

Bouxsein M, Boyd S. 2010. Guidelines for assessment of bone microstructure in rodents using micro–computed tomography. *J bone …* **25**:1468–86. doi:10.1002/jbmr.141

Cheloha RW, Gellman SH, Vilardaga JP, Gardella TJ. 2015. PTH receptor-1 signalling - Mechanistic insights and therapeutic prospects. *Nat Rev Endocrinol*. doi:10.1038/nrendo.2015.139

De Angelis E, Pecoraro M, Rusciano MR, Ciccarelli M, Popolo A. 2019. Cross-talk between neurohormonal pathways and the immune system in heart failure: A review of the literature. *Int J Mol Sci*. doi:10.3390/ijms20071698

DeMambro VE, Maile L, Wai C, Kawai M, Cascella T, Rosen CJ, Clemmons D. 2012. Insulin-

like growth factor-binding protein-2 is required for osteoclast differentiation. *J Bone Min Res* **27**:390–400. doi:10.1002/jbmr.545

Dempster DW, Compston JE, Drezner MK, Glorieux FH, Kanis JA, Malluche H, Meunier PJ, Ott SM, Recker RR, Parfitt AM. 2013. Standardized Nomenclature, Symbols, and Units for Bone Histomorphometry: A 2012 Update of the Report of the ASBMR Histomorphometry Nomenclature Committee. *J Bone Min Res* **28**:2–17. doi:10.1002/jbmr.1805

Ducy P, Amling M, Takeda S, Priemel M, Schilling AF, Beil FT, Shen J, Vinson C, Rueger JM, Karsenty G. 2000. Leptin inhibits bone formation through a hypothalamic relay: a central control of bone mass. *Cell* **100**:197–207.

Elefteriou F, Ahn JD, Takeda S, Starbuck M, Yang X, Liu X, Kondo H, Richards WG, Bannon TW, Noda M, Clement K, Vaisse C, Karsenty G. 2005. Leptin regulation of bone resorption by the sympathetic nervous system and CART. *Nature* **434**:514–520. doi:10.1038/nature03398

Esen E, Lee SY, Wice BM, Long F. 2015. PTH Promotes Bone Anabolism by Stimulating Aerobic Glycolysis via IGF Signaling. *J Bone Miner Res*. doi:10.1002/jbmr.2556

Fan Y, Hanai JI, Le PT, Bi R, Maridas D, DeMambro V, Figueroa CA, Kir S, Zhou X, Mannstadt M, Baron R, Bronson RT, Horowitz MC, Wu JY, Bilezikian JP, Dempster DW, Rosen CJ, Lanske B. 2017. Parathyroid Hormone Directs Bone Marrow Mesenchymal Cell Fate. *Cell Metab* **25**:661–672. doi:10.1016/j.cmet.2017.01.001

Gesty-Palmer D, Luttrell LM. 2011. "Biasing" the parathyroid hormone receptor: A novel anabolic approach to increasing bone mass? *Br J Pharmacol*. doi:10.1111/j.1476-5381.2011.01450.x

Hanyu R, Wehbi VL, Hayata T, Moriya S, Feinstein TN, Ezura Y, Nagao M, Saita Y, Hemmi H,

743 Notomi T, Nakamoto T, Schipani E, Takeda S, Kaneko K, Kurosawa H, Karsenty G,
744 Kronenberg HM, Vilardaga JP, Noda M. 2012. Anabolic action of parathyroid hormone
745 regulated by the beta2-adrenergic receptor. *Proc Natl Acad Sci U S A* **109**:7433–7438.
746 doi:10.1073/pnas.1109036109
747 Jean-Alphonse FG, Wehbi VL, Chen J, Noda M, Taboas JM, Xiao K, Vilardaga JP. 2017. β 2 -
748 adrenergic receptor control of endosomal PTH receptor signaling via Gβ 3. *Nat Chem Biol*.
749 doi:10.1038/nchembio.2267
750 Kajimura D, Hinoi E, Ferron M, Kode A, Riley KJ, Zhou B, Guo XE, Karsenty G. 2011. Genetic
751 determination of the cellular basis of the sympathetic regulation of bone mass accrual. *J Exp*
752 *Med*. doi:10.1084/jem.20102608
753 Khosla S, Monroe DG, Farr JN. 2018. Sympathetic b 1 -adrenergic signaling contributes to
754 regulation of human bone metabolism Graphical abstract Find the latest version : *J Clin*
755 *Invest*.
756 Kondo H, Takeuchi S, Togari A. 2013. beta-Adrenergic signaling stimulates osteoclastogenesis
757 via reactive oxygen species. *Am J Physiol Endocrinol Metab* **304**:E507-15.
758 doi:10.1152/ajpendo.00191.2012
759 Mach DB, Rogers SD, Sabino MC, Luger NM, Schwei MJ, Pomonis JD, Keyser CP, Clohisy
760 DR, Adams DJ, O'Leary P, Mantyh PW. 2002. Origins of skeletal pain: sensory and
761 sympathetic innervation of the mouse femur. *Neuroscience* **113**:155–166.
762 Moriya S, Hayata T, Notomi T, Aryal S, Nakamaoto T, Izu Y, Kawasaki M, Yamada T,
763 Shirakawa J, Kaneko K, Ezura Y, Noda M. 2015. PTH regulates β2-adrenergic receptor
764 expression in osteoblast-like MC3T3-E1 cells. *J Cell Biochem*. doi:10.1002/jcb.24953
765 Motyl KJ, Beauchemin M, Barlow D, Le PT, Nagano K, Treyball A, Contractor A, Baron R,

766 Rosen CJ, Houseknecht KL. 2017. A novel role for dopamine signaling in the pathogenesis
767 of bone loss from the atypical antipsychotic drug risperidone in female mice. *Bone*
768 **103**:168–176. doi:10.1016/j.bone.2017.07.008
769 Motyl KJ, Bishop KA, Demambro VE, Bornstein SA, Le P, Kawai M, Lotinun S, Horowitz MC,
770 Baron R, Bouxsein ML, Rosen CJ. 2013. Altered thermogenesis and impaired bone
771 remodeling in Misty mice. *J Bone Miner Res* **28**. doi:10.1002/jbmr.1943
772 Motyl KJ, DeMambro VE, Barlow D, Olshan D, Nagano K, Baron R, Rosen CJ, Houseknecht
773 KL. 2015. Propranolol attenuates risperidone-induced trabecular bone loss in female mice.
774 *Endocrinology* **156**. doi:10.1210/en.2015-1099
775 Motyl KJ, Dick-de-Paula I, Maloney AE, Lotinun S, Bornstein S, de Paula FJA, Baron R,
776 Houseknecht KL, Rosen CJ. 2012. Trabecular bone loss after administration of the second-
777 generation antipsychotic risperidone is independent of weight gain. *Bone* **50**.
778 doi:10.1016/j.bone.2011.08.005
779 Ortuno MJ, Robinson ST, Subramanyam P, Paone R, Huang YY, Guo XE, Colecraft HM, Mann
780 JJ, Ducy P. 2016. Serotonin-reuptake inhibitors act centrally to cause bone loss in mice by
781 counteracting a local anti-resorptive effect. *Nat Med* **22**:1170–1179. doi:10.1038/nm.4166
782 Osima M, Borgen TT, Lukic M, Grimnes G, Joakimsen RM, Eriksen EF, Bjørnerem. 2018.
783 Serum parathyroid hormone is associated with increased cortical porosity of the inner
784 transitional zone at the proximal femur in postmenopausal women: the Tromsø Study.
785 *Osteoporos Int*. doi:10.1007/s00198-017-4298-3
786 Pierroz DD, Bouxsein ML, Rizzoli R, Ferrari SL. 2006. Combined treatment with a beta-blocker
787 and intermittent PTH improves bone mass and microarchitecture in ovariectomized mice.
788 *Bone* **39**:260–267. doi:10.1016/j.bone.2006.01.145

789 Rodrigues WF, Madeira MFM, da Silva TA, Clemente-Napimoga JT, Miguel CB, Dias-da-Silva
790 VJ, Barbosa-Neto O, Lopes AH, Napimoga MH. 2012. Low dose of propranolol down-
791 modulates bone resorption by inhibiting inflammation and osteoclast differentiation. *Br J*
792 *Pharmacol* **165**:2140–2151. doi:10.1111/j.1476-5381.2011.01686.x
793 Sozzani S, Agwu DE, McCall CE, O'Flaherty JT, Schmitt JD, Kent JD, McPhail LC. 1992.
794 Propranolol, a phosphatidate phosphohydrolase inhibitor, also inhibits protein kinase C. *J*
795 *Biol Chem*.
796 Takeda S, Elefteriou F, Levasseur R, Liu X, Zhao L, Parker KL, Armstrong D, Ducy P, Karsenty
797 G. 2002. Leptin regulates bone formation via the sympathetic nervous system. *Cell*
798 **111**:305–317.
799 Takigawa S, Chen A, Wan Q, Na S, Sudo A, Yokota H, Hamamura K. 2016. Role of miR-222-
800 3p in c-Src-Mediated Regulation of Osteoclastogenesis. *Int J Mol Sci*.
801 doi:10.3390/ijms17020240
802 Tinajero JC, Fabbri A, Dufau ML. 1993. Serotonergic inhibition of rat leydig cell function by
803 propranolol. *Endocrinology*. doi:10.1210/endo.133.1.8391422
804 Toulis KA, Hemming K, Stergianos S, Nirantharakumar K, Bilezikian JP. 2014. β-adrenergic
805 receptor antagonists and fracture risk: A meta-analysis of selectivity, gender, and site-
806 specific effects. *Osteoporos Int*. doi:10.1007/s00198-013-2498-z
807 Vengellur A, LaPres JJ. 2004. The role of hypoxia inducible factor 1α in cobalt chloride induced
808 cell death in mouse embryonic fibroblasts. *Toxicol Sci*. doi:10.1093/toxsci/kfh278
809 Wheeler D, Sneddon WB, Wang B, Friedman PA, Romero G. 2007. NHERF-1 and the
810 cytoskeleton regulate the traffic and membrane dynamics of G protein-coupled receptors. *J*
811 *Biol Chem*. doi:10.1074/jbc.M701544200

812 Yadav VK, Oury F, Suda N, Liu ZW, Gao XB, Confavreux C, Klemenhagen KC, Tanaka KF,
813 Gingrich JA, Guo XE, Tecott LH, Mann JJ, Hen R, Horvath TL, Karsenty G. 2009. A
814 serotonin-dependent mechanism explains the leptin regulation of bone mass, appetite, and
815 energy expenditure. *Cell* **138**:976–989. doi:10.1016/j.cell.2009.06.051
816 Yang S, Nguyen ND, Eisman JA, Nguyen T V. 2012. Association between beta-blockers and
817 fracture risk: A Bayesian meta-analysis. *Bone*. doi:10.1016/j.bone.2012.07.013
818 Yirmiya R, Goshen I, Bajayo A, Kreisel T, Feldman S, Tam J, Trembovler V, Csernus V,
819 Shohami E, Bab I. 2006. Depression induces bone loss through stimulation of the
820 sympathetic nervous system. *Proc Natl Acad Sci U S A* **103**:16876–16881.
821 doi:10.1073/pnas.0604234103
822 Zayzafoon M, Fulzele K, McDonald JM. 2005. Calmodulin and calmodulin-dependent kinase IIα
823 regulate osteoblast differentiation by controlling c-fos expression. *J Biol Chem*.
824 doi:10.1074/jbc.M412680200
825 Zebaze R, Takao-Kawabata R, Peng Y, Zadeh AG, Hirano K, Yamane H, Takakura A, Isogai Y,
826 Ishizuya T, Seeman E. 2017. Increased cortical porosity is associated with daily, not
827 weekly, administration of equivalent doses of teriparatide. *Bone*.
828 doi:10.1016/j.bone.2017.03.042
829

Supplemental References

Ide N, Ye R, Courbebaisse M, Olauson H, Densmore MJ, Larsson TE, Hanai JI, Lanske B. 2018. In vivo evidence for an interplay of FGF23/Klotho/PTH axis on the phosphate handling in renal proximal tubules. *Am J Physiol - Ren Physiol*. doi:10.1152/ajprenal.00650.2017

Irwin R, Lee T, Young VB, Parameswaran N, McCabe LR. 2013. Colitis-induced bone loss is gender dependent and associated with increased inflammation. *Inflamm Bowel Dis* **19**:1586–1597. doi:10.1097/MIB.0b013e318289e17b

Li J, Takaishi K, Cook W, McCorkle SK, Unger RH. 2003. Insig-1 "brakes" lipogenesis in adipocytes and inhibits differentiation of preadipocytes. *Proc Natl Acad Sci U S A*. doi:10.1073/pnas.1133426100

Motyl KJ, DeMambro VE, Barlow D, Olshan D, Nagano K, Baron R, Rosen CJ, Houseknecht KL. 2015. Propranolol attenuates risperidone-induced trabecular bone loss in female mice. *Endocrinology* **156**. doi:10.1210/en.2015-1099

Ontiveros C, Irwin R, Wiseman RW, McCabe LR. 2004. Hypoxia suppresses runx2 independent of modeled microgravity. *J Cell Physiol* **200**:169–176. doi:10.1002/jcp.20054

Ontiveros C, McCabe LR. 2003. Simulated microgravity suppresses osteoblast phenotype, runx2 levels and AP-1 transactivation. *J Cell Biochem*. doi:10.1002/jcb.10410

Vengellur A, LaPres JJ. 2004. The role of hypoxia inducible factor 1α in cobalt chloride induced cell death in mouse embryonic fibroblasts. *Toxicol Sci*. doi:10.1093/toxsci/kfh278

Wiren KM, Zhang XW, Toombs AR, Kasparcova V, Gentile MA, Harada SI, Jepsen KJ. 2004. Targeted overexpression of androgen receptor in osteoblasts: Unexpected complex bone phenotype in growing animals. *Endocrinology*. doi:10.1210/en.2003-1016